Spring 5-4-2019

Synthesis and Characterization of a Long-Acting Emtricitabine Prodrug Nanoformulation

Ibrahim M. Ibrahim
University of Nebraska Medical Center

SYNTHESIS AND CHARACTERIZATION OF A LONG-ACTING EMTRICITABINE PRODRUG NANOFORMULATION

By

Ibrahim M. Ibrahim

A DISSERTATION

Presented to the Faculty of the University of Nebraska Medical Center Graduate College
in Partial Fulfillment of the Requirements for the Degree of Doctor of Philosophy

Pharmacology and Experimental Neuroscience Graduate Program

Under Supervision of Professor Howard E. Gendelman

University of Nebraska Medical Center
Omaha, NE

May, 2019

Supervisory Committee

JoEllyn McMillan, PhD   Santhi Gorantla, PhD

Myron Toews, PhD   Yazen Alnouti, PhD

SYNTHESIS AND CHARACTERIZATION OF A LONG-ACTING EMTRICITABINE PRODRUG FORMULATION

Ibrahim M. Ibrahim, MBBS, PhD

University of Nebraska Medical Center, 2019

Supervisor: Howard E. Gendelman, MD

The introduction of highly active antiretroviral therapy led to a paradigm shift in the management of HIV/AIDS changing a disease considered "a death sentence" to "a manageable chronic disease". Nevertheless, challenges exist for successful treatment of HIV, including patient adherence to the complex daily regimens and the inability of current formulations to target viral sanctuaries. Introduction of nanoformulated antiretroviral therapy (ART) is a promising alternative to tackle these challenges. Our laboratory has been focusing on developing long-acting (LA) nanoformulated antiretrovirals and has succeeded in developing LA integrase inhibitors. However, challenges for this approach extend to a range of short-acting hydrophilic drugs, mainly nucleoside reverse transcriptase inhibitors (NRTIs). To this end, we developed a one-step synthesis scheme to create a hydrophobic ester prodrug of emtricitabine (FTC), an NRTI that is a key component of the initial ART and of a reported pre-exposure prophylaxis measure. The nanoformulation process was optimized to prepare poloxamer 407-encased nanocrystals. To eliminate HIV from the viral sanctuaries, macrophages were harnessed as "Trojan horses" for drug delivery and distribution to these difficult-to-reach sanctuaries. Nanoformulation of the FTC prodrug was facilitated by conjugating it to a long fatty acid chain, palmitoyl chloride. The resultant nanoparticles exhibited long-term stability, higher uptake and longer retention in macrophages, and these properties were translated into extended antiretroviral efficacy for 10 days. Moving this nanoformulation forward into

animal studies showed sustained FTC blood concentrations of more than 20-times its EC_{50} at day 7 after a single intramuscular injection in rats, in contrast to undetectable levels following parent FTC injection. Furthermore, higher concentrations of FTC were observed in liver, spleen lymph nodes, and brain tissues. Interestingly, these results were mirrored by intracellular FTC triphosphate levels that were detectable for up to 10 days in vitro, and for 7 days in peripheral blood mononuclear cells (PBMCs) and in cells isolated from spleen and lymph nodes. We anticipate that this nanoformulation will further extend drug action in humans considering reported species differences in plasma esterase activities. Also, these improvements aided by medicinal chemistry unveils new opportunities for LA FTC formulation and for other NRTIs as well. These simplified manufacturing strategies hold promises for bringing LA ART closer to clinical translation.

Acknowledgments

First, I would like to give my sincere gratitude to my mentor Dr. Howard E Gendelman, for his constant support and guidance. Dr. Gendelman not only provided all the resources that could lead to my success, but also inspired me with his hard work, perseverance, and enthusiasm in science. I was told once that top universities are at this level because they have outstanding students. However, after joining Dr. Gendelman's lab, I realized that you only need an outstanding mentor to become successful and to do great science even if he is in Nebraska. From him, I learnt not only how to become a scientist, but also how to become a good family person. He never held me back when my family needed me, and always answered his mother's call even during lab meetings. Also, he has been a role model for me to maintain my health. If Dr. Gendelman is reading this, I would like to share with him that I rode my bicycle from home to UNMC non-stop 11-mile round trip.

Next, I would like to express my sincere gratitude to Dr. Benson Edagwa for being there whenever I needed him. He taught me not only the knowledge and skills I needed in chemistry, but always advised me to keep my family my first priority.

I would also like to thank my graduate supervisory committee members Drs. JoEllyn McMillan, Myron Toews, Yazen Alnouti, and Santhi Gorantla for their valuable support and guidance during my journey for PhD. I would like to thank Dr. McMillan for her continuous support and for fostering my research skills. I thank Dr. Toews for his guidance and teachings to perfect my slide presentations and my scientific writing skills. I thank Dr Alnouti and Nagsen Gautam for developing LC-MS/MS method to quantifying FTC-TP, and for data analysis.

I was so lucky to work with wonderful team from Dr. Gendelman's lab. I would like to thank Drs. Aditya Bade, Prasanta Dash, Mariluz Arainga Ramirez, and Hang Su for their help and guidance in animal studies; I thank Melinda and Bhagya Laxmi Dyavar Shetty for UPLC-MS/MS analyses. I would also like to thank Dr. Bhavesh Kevadiya, Mary Banoub, Insiya Mukaddam, Mahmudul Hasan, Brendan Ottemann, Jonathan Herskovitz, Marwa Mohamed, James Hilaire, Denise Cobb, Brady Sillman, Dhruvkumar Soni, Nathan Smith, Zhiyi Lin, and Tanmay Kulkarni not for only helping and teaching me the biological assays, but also for providing me a healthy friendly environment for me to work in.

I would also like to thank the Saudi Arabian Cultural Mission for the financial support all these years. I thank the administrative staff of the department of pharmacology and experimental neuroscience for making my life easier. I also thank all UNMC core facility including animal facility personnel for their cooperation.

I would like to express my sincere gratitude to my parents, my late father Mohammad Ayoub, and my mother Sabirah Alhindi for raising me, taking care of me till I became a grown up, and for supporting me till I became a medical doctor. Although they were not highly educated, they were always willing to sacrifice everything for me and my siblings' education and brighter future. May God rest my father's soul in eternal peace and grant my mother health and all the happiness in life.

I am extremely grateful for my joy of life, my wife Bushra and my lovely kids Kayan, Ilyan, and Armaan for giving me happiness and a new purpose of life. With them I realized that my home is wherever they are with me. I specially thank my wife for her love and support, and for taking good care of our children during my absence. She always guided me to become a good father and a good husband as well. We had been together in many hardships during our long journey here in USA, away from our families but every hardship made our relationship even stronger. I am so grateful to God for these invaluable bounties.

Last but not the least, I would like to thank our family friends here in Omaha. Without whom our life would have become tasteless. I owe a special thanks to Ragda Mukbel for taking good care of our children, and for being a friend, a sister, and a mother for us.

Ibrahim M. Ibrahim

University of Nebraska Medical Center

May 2019

Table of Contents

List of Figures

List of Tables

List of Abbreviations

3TC	Lamivudine
AIDS	Acquired immunodeficiency virus
ART	Antiretroviral therapy
ARV	Antiretroviral drug
ATV	Atazanavir
CAB	Cabotegravir
CCK-8	Cell counting kit-8
CDC	Centers for disease control and prevention
C_{max}	Maximum concentration
DAB	3,3`-diaminobenzidine
DCM	Dichloromethane
DLS	Dynamic light scattering
DMEM	Dulbecco's Modified Eagle's Medium
DMSO	Dimethyl sulfoxide
EC_{50}	Half maximum effective concentration
EO	Ethylene oxide
FDA	Food and drug administration
FTC	Emtricitabine
FTC-TP	Emtricitabine triphosphate

HBSS	Hank's Balanced salt solution
HEPES	4-(2-hydroxyethyl)-1-piperazineethanesulfonic acid
HIV	Human immunodeficiency virus
HLA	Human leukocyte antigen
HLB	Hydrophilic-lipophilic balance
HPLC	High-performance liquid chromatography
HSC	Human stem cell
IL-2	Interleukin-2
IM	Intramuscular
KCl	Potassium chloride
LA	Long-acting
LASER ART	Long-acting slow effective release antiretroviral therapy
MDM	Monocyte-derived macrophage
MFTC	Modified emtricitabine prodrug
MOI	Multiplicity of infection
MS/MS	Tandem mass spectrometry
NATV	Nanoformulated atazanavir
NK	Natural killer
NMFTC	Nanoformulated MFTC
NMR	Nuclear magnetic resonance

NNRTI	Non-nucleoside reverse transcriptase inhibitor
NOD	Non-obese diabetic
NRTI	Nucleoside reverse transcriptase inhibitor
P188	Poloxamer 188
P237	Poloxamer 237
P238	Poloxamer 238
P338	Poloxamer 338
P403	Poloxamer 403
P407	Poloxamer 407
PBL	Peripheral blood lymphocyte
PBMC	Peripheral blood mononuclear cell
PBS	Phosphate buffer saline
PCR	Polymerase chain reaction
PD	Pharmacodynamics
PDI	Polydispersity index
PFA	Paraformaldehyde
PK	Pharmacokinetics
PO	Propylene oxide
PrEP	Pre-exposure prophylaxis
RPV	Rilpivirine

RT	Reverse transcriptase
SD	Standard deviation
SEM	Standard error of the mean
SHIV	Simian/human immunodeficiency virus
t1/2	Half-life
^{t}BuMgCl	Tert-butylmagnesium chloride
TCID	Tissue culture infectious dose
TDF	Tenofovir disoproxil fumarate
TEM	Transmission electron microscopy
THF	Tetrahydrofuran
UNMC	University of Nebraska Medical Center
UPLC	Ultra-performance liquid chromatography
XRD	X-ray diffraction

Chapter I. Introduction

1.1 HIV & AIDS Pandemic

The extent of human immunodeficiency virus (HIV) infection is considerably variable between regions and countries. Although HIV has spread worldwide, African regions remains the most severely affected, with nearly 1 in every 25 adults is infected, and accounting for two thirds of the people infected with HIV globally [1]. According to statistical data available from UNAIDS for 2017, 36.9 million people were surviving with HIV. Of those, 1.8 million were newly infected, bringing the number of infected people since the start of the epidemic to 77.3 million. More concerning, only 21.7 million infected people had access to antiretroviral therapy (ART). Sadly, 940,000 people died due to AIDS-related illnesses including infections and cancers, bringing the number of deaths from HIV since the start of the epidemic to 35.4 million. At the end of 2017, there were 21.3 billion US dollars available for the AIDS response in low- and middle- income countries. However, it is estimated that the fund required for the same cause will increase to 26.2 billion US dollars in 2020 [2].

1.2 HIV Biology

Acquired immunodeficiency syndrome (AIDS) was first reported by the United States Centers for Disease Control and Prevention (CDC) among homosexual men in New York and California in 1981 after observing increasing cases of rare diseases especially opportunistic infections and persistent lymphadenopathy [3, 4]. After a couple of years in 1983, the causative agent was discovered and named Human T Lymphocyte Virus (HTLV-III) until it acquired the current name as Human Immunodeficiency Virus (HIV) [5, 6]. HIV was found to be different in structure than other retroviruses. The HIV virion is about 100 nm in diameter. Its cone-shaped core consists of two copies of its ssRNA genome; the enzymes reverse transcriptase (RT), integrase, and protease; and several minor and major core proteins. The viral genome encodes 16 proteins that play

essential roles in the viral life cycle [7]. Advances in x-ray crystallography, cryo-electron microscopy, and cryo-electron tomography came together to study and describe the HIV envelope that facilitates viral interaction with host cell CD4 receptors and co-receptors CCR5 and CXCR4 [8-10]. The HIV envelope is a trimer containing three copies of non-covalently associated heterodimers of gp120, the component that interacts with host cell receptors, and gp41, the transmembrane component essential for viral fusion with the cellular target membrane. Beside facilitating viral entry, the viral envelop plays a major role in evading host immune system. It also contributes to development of drug resistance against ART because of heterogeneity of the envelope that undergoes constant mutations of the envelope proteins [11].

1.3 HIV Pathogenesis

HIV infection in the host begins by the binding of the viral envelope to the CD4 receptor and/or co-receptors CCR5 or CXCR4 on the cell surface. This interaction results in fusion of the viral and host cell membranes facilitating entry of the viral capsid core into the cytoplasm. Here, the viral RT begins to convert its RNA genome into double-stranded DNA. The core capsid then traffics into the host cell nucleus where it utilizes nuclear machinery to form progeny virions that are ultimately released to target new cells and propagate the infection (Figure 1) [12].

HIV is a sexually transmitted disease that gains access through the mucosal membranes of the vagina, vulva, penis, and rectum. HIV is also spread by contact with infected blood, commonly among drug abusers through exchanging needles or syringes [13]. Although very low, risk of infection among health care providers also exists [14] with the risk estimated to be 0.3% after a needlestick and 0.09% after mucosal membrane exposure [15].

The course of infection with HIV is characterized by a long viral incubation period that may extend to more than 10 years before the onset of serious symptoms [16]. During the course of the disease, the patient generally starts suffering from flu-like illness and rash. With disease progression, as HIV continues replicating slowly, and infecting more CD4 lymphocyte and other cells, including monocytes and thymocytes [17, 18], the patient's immune system deteriorates gradually. Normally, a healthy individual has CD4$^+$ cell counts of 800-1200 cells/mm^2. As CD4$^+$ cells are destroyed by HIV, and the cell count drops to <500 cells/mm^2, minor infections such as cold sores (herpes simplex) and vaginal candidiasis may occur. These infections are concerning but not life threatening. When CD4$^+$ counts drop below 200 cells/mm^2, the patient becomes vulnerable to serious opportunistic infections and the cancers that are the hallmarks of AIDS, the end stage of HIV (Figure 2) [19].

1.4 Current anti-HIV Therapy

Currently available ART is prescribed as a combination of drugs that target multiple stages of the HIV life-cycle. These drugs have significantly improved disease outcomes, a death sentence at one time, by reducing viral load and maintaining adequate CD4$^+$ lymphocyte counts. Thus, decreased morbidity and mortality rates and limited viral transmission now render HIV a chronic disease. According to the International Antiviral Society-USA Panel, the recommended initial therapy includes two nucleoside reverse transcriptase inhibitors (NRTIs) and an integrase or a non-nucleoside reverse transcriptase inhibitor (NNRTI) [20]. However, additional classes of ART have been developed in response to emergence of drug resistance, drug-related toxicity, and other complications. These include, entry inhibitors, protease inhibitors, and integrase inhibitors. The chemical structures of different classes of drugs used in ART are illustrated in Figure 3.

1.4.1 Entry inhibitors

As described earlier that viral entry into host cell requires binding of viral envelope proteins to a cellular receptor CD4 and a co-receptor, CCR5 or CXCR4. Entry inhibitors act by interfering with this interaction being the only class that acts before the infection. There are only two drugs approved in this class, maraviroc and enfuvirtide. Maraviroc acts by targeting host cell antagonizing CCR5 that binds viral gp120 envelope protein. Whereas enfuvirtide targets viral gp41 [21].

1.4.2 Nucleoside/nucleotide reverse transcriptase inhibitors

Several NRTIs were approved by US Food and Drug Administration (FDA) including abacavir, emtricitabine (FTC), lamivudine (3TC), and tenofovir. These drugs have to be activated in the cell to their active triphosphate metabolite to compete with intrinsic nucleosides for incorporation into the elongating viral DNA. Once incorporated, these nucleoside analogues lack a 3'-hydroxyl group that interacts with the next coming nucleoside terminating viral RT; thus, DNA synthesis. NRTIs are generally well tolerated; however, most commonly reported toxicities are ascribed to mitochondria as NRTIs are capable of inhibiting mitochondrial DNA synthesis, which may result in myopathy, peripheral neuropathy, pancreatitis, and lactic acidosis [22, 23].

1.4.3 Non-nucleoside reverse transcriptase inhibitors

The NNRTI act by binding non-competitively to the RT enzyme. The binding causes conformational change in the three-dimensional structure of the enzyme [24]. First-generation NNRTIs include nevirapine, delavirdine, and efavirenz. These drugs have low genetic barrier and poor resistance profile, which led to the development of the second-generation of NNRTIs. The new generation includes etravirine and rilpivirine.

1.4.4 Integrase inhibitors

Integrase inhibitors act by interfering with insertion of viral genome into host cell genome by blocking the binding of the preintegration complex to cellular DNA. Clinically approved integrase inhibitors include dolutegravir, cabotegravir (CAB), elvitegravir, and raltegravir. Integrase inhibitor are generally well tolerated and are recommended as part of initial HIV therapy along with 2 NRTIs.

1.4.5 Protease inhibitors

Protease inhibitors act by inhibiting cleavage of the viral gag and gag-pol protein precursors into functional proteins, blocking nascent virion maturation and its infectivity [25]. There are several approved protease inhibitors such as, atazanavir and darunavir, that are commonly used in combination with low-dose ritonavir as a booster due to its ability to inhibit CYP3A4 slowing down the metabolism of the protease inhibitors [26].

1.4.6 ART-associated challenges

Development of viral drug resistance was a major challenge during early use of ARTs. This was attributed to the high mutation rate of the viral genome during active replication, limiting the effectiveness of monotherapy. Therefore, combination ART (cART) was employed targeting multiple stages of the viral life-cycle. Effective treatment of HIV requires lifelong administration cART with near perfect adherence as patient non-adherence is the main cause of treatment failure. Factors associated with patient non-adherence include: 1) factors related to treatment regimens as more complex regimens are associated with decreased adherence; 2) social and emotional status of the patient and availability of health care provider support; 3) personal factors related to younger age, minority status, and frequent history of substance abuse [27]. Rapid viral rebound due to non-adherence has been attributed to HIV latency where current drugs are not effective due to slow viral replication. Additionally, this slow replication during latency can occur in

HIV cellular and/or anatomical reservoirs where current formulations do not have access [28, 29].

Among cellular reservoirs, memory CD4^{+} T cells, including both transitional (CD45RA-CCR7-CD27+) and central (CD45RA-CCR7+CD27+) T cells, one of the sources of persistent latency. Naïve CD4^{+} T cells have also been reported as sites of HIV latency, although at much lower intensity than memory T cells. Recently, integrated HIV DNA has been detected in CD34^{+} hematopoietic progenitor cells from 40% of patients under cART [30]. Also, astrocytes isolated from HIV-infected patients showed the presence of integrated HIV DNA, which has been linked to HIV-associated dementia. However, this finding was in patients exhibiting active viremia, and further studies on patients under cART are required. Furthermore, monocyte-macrophages have been reported as HIV reservoirs. However, to lesser extent than CD4^{+} T cells that is attributed to lower CD4 expression on macrophages, and to restrictions in nuclear import and reverse transcription resulting in limited infection [30].

Several anatomical reservoirs have been reported with gastrointestinal tract being the most prominent reservoir with five- to ten-fold higher viral load than PBMCs. Infected CD4^{+} T cells carrying the viral genome through the lymphatic circulation renders lymphoid tissue an important reservoir. Moreover, follicular dendritic cells residing in the germinal center may provide a stable source of latent virus. HIV RNA has been detected in genitourinary tract of 54% of women and in semen of 8 to 10% of men on suppressive cART, indicating a reservoir in the genital tracts. Furthermore, the blood-testis barrier restricts the entry of immune cells, providing a niche for viral latency [31, 32].

1.5 Long-acting antiretroviral therapy

Long-acting (LA) formulations have proven to be very successful in diverse areas of medicine including, contraception [33], type 2 diabetes [34], psychotic diseases, neuroendocrine tumors [35] and many others. Furthermore, there are considerable efforts to generate LA antimalarial [36] and anti-tuberculous drugs [37]. In the case of second-generation LA antipsychotics, several formulations are available in clinical practice that have shown to be superior to their oral counterparts. Interestingly, a 3-monthly injection formulation of paliperidone has been approved and it is a first LA injectable agent to extend the dosing regimen beyond the typical monthly regimen [38]. LA formulations have the advantage of improving patient adherence, reducing risk of overdose and accidental poisoning, and increasing drug bioavailability for those with difficulty absorbing oral medications. In contrast to daily regimens, LA formulations offer sustained plasma drug levels reducing the risk of drug level falling below its therapeutic window, which commonly occurs with missed doses; thus, reducing the risk of acquiring drug resistance (Figure 4). Additionally, LA drugs offer a means for differentiating between lack of efficacy and lack of adherence. incomplete adherence to anti-HIV therapy has been a concerning issue for both HIV treatment and prevention. To answer the question of willingness of patients to switch to LA drugs instead of once daily regimens, a survey was conducted where 74% of 400 HIV infected patients reported that they would consider switching to LA ART [39]. However, adherence is even more concerning in healthy at high-risk population due to, beside not having the disease, their concern of being mistakenly recognized as HIV positive [40].

1.5.1 Challenges associated with LA ART

A critical challenge in developing LA ART, to be administered once monthly for example, is drug loading capacity. As an example, for the FTC studied in this project, the

drug is dosed orally at 200 mg once daily. To make a monthly injection, therefore, the drug delivery platform should be capable of encapsulating 6 g of FTC (a 30-day supply) in a reasonable injection volume. Therefore, the potency of the candidate drug along with the drug delivery system are critical for making LA ART clinically feasible. Most of the therapeutic agents in LA formulations are hydrophobic, posing an additional challenge compared to hydrophilic drugs, such as NRTIs and maraviroc [41]. In addition to the physical characteristics of the drug, changing the route of administration from oral to intramuscular (IM) or subcutaneous (SC) would affect drug absorption, distribution, and metabolism, all of which require thorough investigation and optimization.

For LA injectables, the most commonly used formulations are oil-based formulations, such as some first-generation antipsychotics, haloperidol decanoate and fluphenazine decanoate [42]. These were composed of insoluble drugs dispersed in oils, such as sesame oil. However, this method is no longer in use due to the high excipient content required. To overcome the limitations of hydrophilic drugs, hydrophobic prodrug strategies have been employed, such as conjugating fatty acid chains to the parent drug or by making hydrophobic salts [43, 44]. As an alternative to oil-based formulations, drug suspensions, or nanosuspensions in particular, have received great attention because they offer higher drug loading capacity, higher biodistribution because of their ability to cross biological membranes such as the blood brain barrier, and due to their improved drug release profiles [45]. Interestingly, the 3-monthly injection mentioned earlier for an antipsychotic was formulated as an aqueous nanosuspension [46]. Taking into account the intrinsic properties of ART, the above-mentioned challenges render most ART drugs not suitable candidates for LA formulations.

1.5.2 Cell-mediated drug delivery systems

Like $CD4^+$ T cells, macrophages have excellent properties as an HIV reservoir. This is due to the long life span of the macrophage -- brain microglia can survive for years

-- and to the fact that macrophages are part of the immune system, which helps the virus evade the immune response. Therefore, targeting macrophages is a major challenge for eradicating HIV. In addition to targeting HIV residing in macrophages, one can utilize these cells as vehicles to deliver drugs to other tissues. This approach offers several advantages that include delivery to the site of infection or inflammation, particularly HIV anatomical reservoirs; prolongation of drug apparent half-life and controlled drug release, thus improving pharmacokinetics (PK); and minimization of drug immunogenicity. Furthermore, the ability of macrophages to cross biological barriers allows them to be used as "Trojan horses" to carry drugs, for example across the blood brain barrier [47].

Despite such advantages, there are several complications for efficient utilization of macrophages as delivery vehicles. These include: 1) loading a high amount of drug; 2) the need for the drug to be protected from intracellular lysosomal degradation; 3) a means to prevent premature release of the drug to ensure delivery at the desired site; 4) preventing the drug from affecting the transmigration abilities of the cells; and 5) ensuring that the drug maintains its cellular biological functions during delivery [47]. To fulfill these requirements, our lab has developed cell-targeted long-acting slow effective release ART (LASER ART). Previous studies have shown that LASER ART is readily taken up by macrophages and forms intracellular depots that can be safely delivered to viral reservoir sites, thus, prolonging drug half-life and improving drug biodistribution and efficacy [48-52].

1.6 Significance of the current project

FTC is an ARV drug used for treatment and prevention of HIV. The drug is a cytidine analogue that must be transformed by the host cell into its active metabolite, FTC triphosphate. It then acts by competing with native nucleoside triphosphates for integration into elongating viral DNA and leads to termination of viral reverse transcription. This drug

was selected for the current project based on its potency, bioavailability, and limited toxicity profile [53]. Furthermore, FTC in combination with tenofovir disoproxil fumarate (TDF), Truvada®, has proven effective as an oral once-daily pre-exposure prophylaxis measure (PrEP) [54]. Thus, creation of an LA FTC formulation should aid in better prevention of HIV because of the non-adherence issues that exist with current PrEP [55]. Therefore, this important drug is an important candidate for conversion to an LA formulation with improved clinical properties.

This study was conducted in four phases. The first was to screen multiple poloxamers for optimization of nanoformulation strategy. The second was synthesizing a hydrophobic prodrug of FTC and its encasement in polymer nanoparticles along with extensive characterization of both the prodrug and the nanoparticle. The third was evaluation of the PK properties of the nanoparticle. The fourth phase investigated the antiretroviral efficacy of the nanoparticle in an *in vivo* animal model.
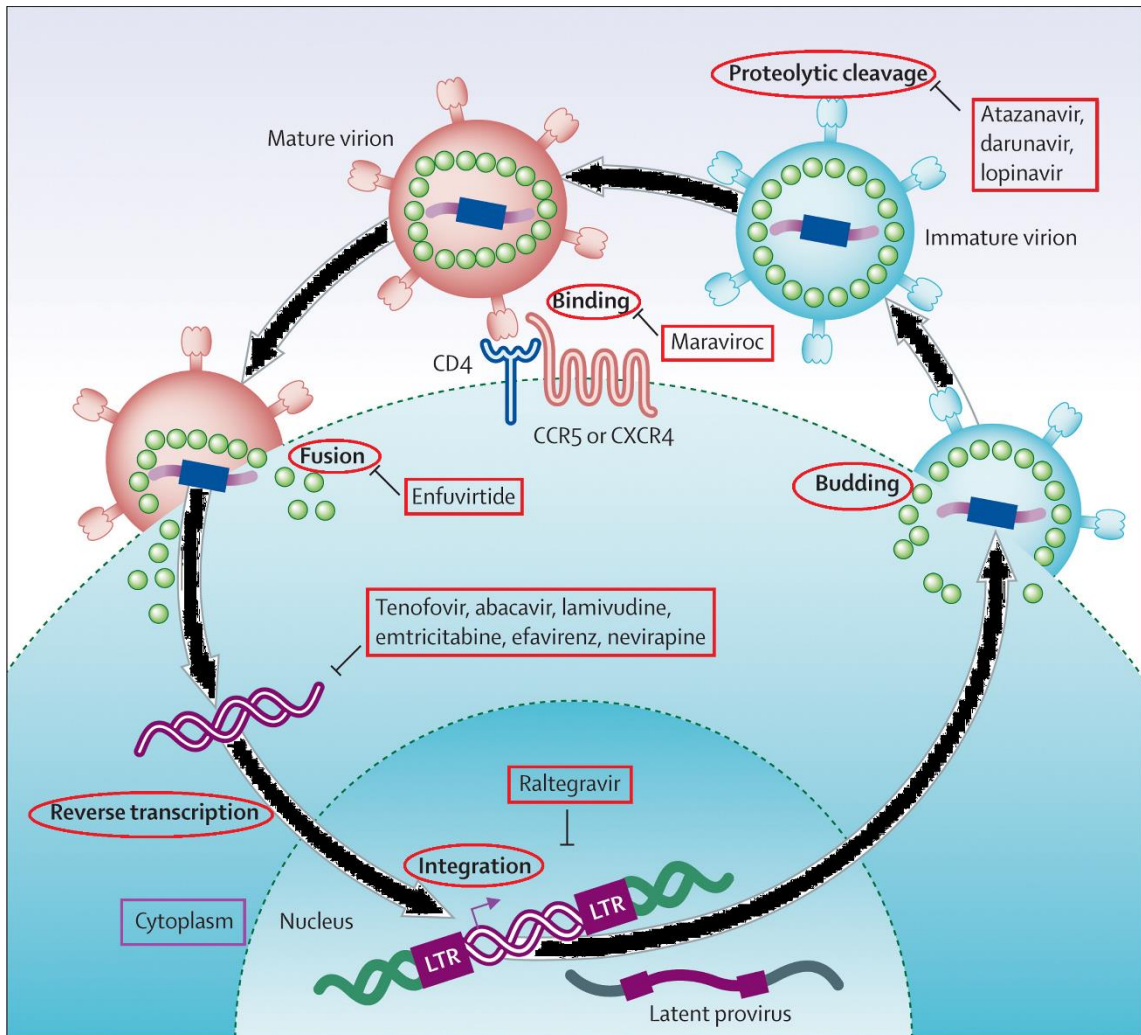
Figure 1.1 HIV-1 life-cycle. The infection begins with interaction of HIV envelope proteins and host cell surface receptors and co-receptors that leads to fusion of viral and cellular membranes. Viral reverse transcription takes place in the cytoplasm before trafficking of the viral capsid into the nucleus where the viral genome integrates into the host cell genome.

The figure was modified from [56]
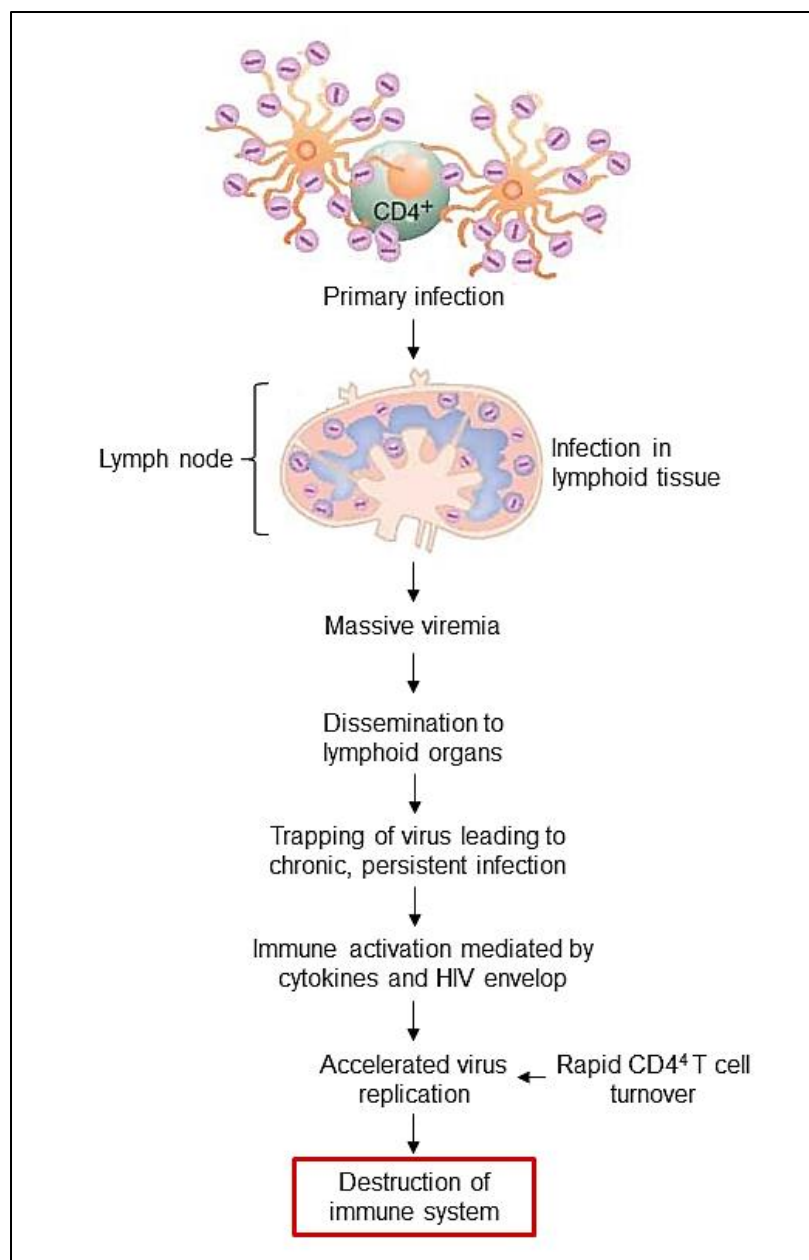
Figure 1.2 HIV pathogenesis. Once HIV is in the body, dendric cells (orange) carry the virus to CD4+ T cells that migrate to lymphoid tissues. The established infection, due to massive viremia, spreads throughout lymphoid tissues. An immune response specific to HIV occurs and traps the virus in the germinal centers of the lymphoid tissue. At this point, despite the immunological response, a chronic, persistent infection is established. Immune activation mediated by cytokines accelerates virus replication which, in association with rapid CD4+ T cell turnover, gradually destroys the host immune system.

The figure was modified from [57].
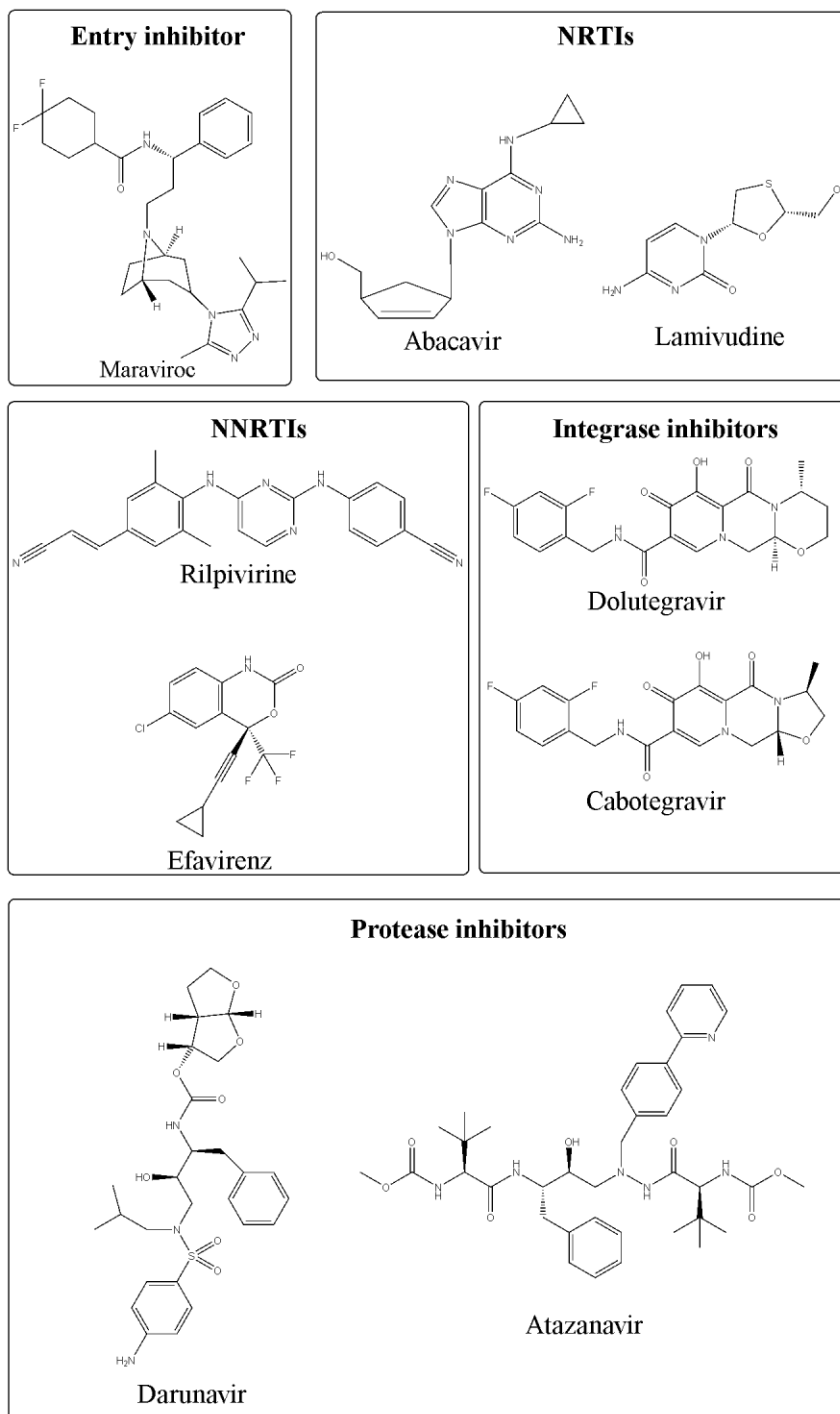
Figure 1.3 Chemical structures of ART. This figure shows examples of different classes of antiretroviral drugs along with their chemical structures.
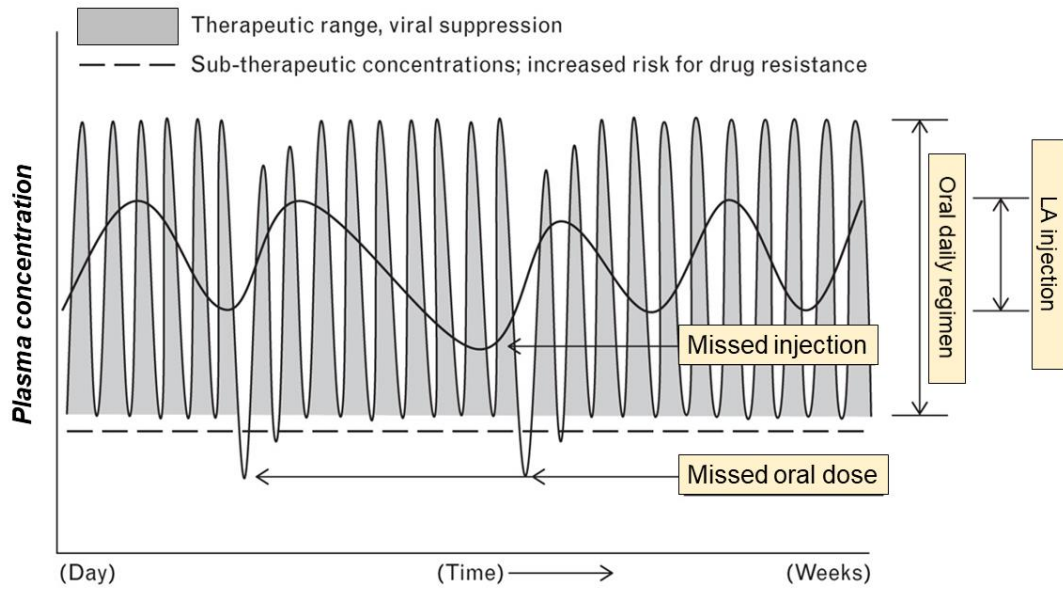
Figure 1.4 Effect of dose fluctuation. Subtherapeutic concentration with an increased

risk of acquiring drug resistance is represented by the dashed line. In contrast, LA injection

maintains steady therapeutic drug concentrations.

The figure is modified from [41].

Chapter II. Poloxamer Screening for Enhanced Stability and Uptake of Nanoformulations

2.1 Abstract

While the need for LA ART is inevitable, targeting HIV cellular and anatomical sanctuaries by drugs able to penetrate into these sites has not yet been realized. Passive macrophage targeting by LA ART could provide a means to optimize a system for drug delivery to viral sanctuaries. However, a challenge to translate such ART rests in optimizing synthesis and formulation with production reproducibility. To this end, our lab has developed a simple, reproducible, and scalable synthesis process for nanoformulated LA ART for passive macrophage targeting. We have demonstrated that this can be achieved by encasing the drug with a polymeric stabilizer, poloxamer 407, that results in stable nanoparticles with high loading capacity. We now further optimize this process aiming for even more stable nanoparticles exhibiting higher uptake by monocyte-derived macrophages. We synthesized and characterized nanoparticles with multiple different poloxamers. The protease inhibitor atazanavir (ATV) was used without any modification, due to its intrinsic hydrophobic property that is essential for making nanoparticles with our method. The manufacturing scheme developed is superior to previously described methods based on greater simplicity and reproducibility of the process. Direct manufacturing provides a path toward large-scale production of macrophage-targeted LA ART.

2.2 Introduction

LA ART has generated great interest in the pharmaceutical industry for the treatment and prevention of HIV infection. LA ART parenteral injections have demonstrated maintenance of plasma drug levels for months, overcoming the patient adherence issue associated with disease management [58]. Combination of LA CAB and rilpivirine (RPV) was the first regimen that demonstrated efficacy and safety comparable to the daily oral three-drug regimen [59]. Both CAB and RPV are highly potent drugs with

low aqueous solubility, allowing them to be formulated as suspensions by wet-milling [60, 61]. However, the high injection volumes required, and injection site reactions were major limitations of this formulation, leading to patients withdrawing from clinical trials. Additionally, the inability of this formulation to penetrate into viral reservoirs limited its therapeutic outcomes [59, 62, 63]. To avoid these limitations, we investigated different poloxamers as surfactants, first to ensure a longer stability nanoformulation in different storage conditions, and second, to enhance drug uptake by monocyte-derived macrophages (MDMs), one of the viral reservoirs and perhaps for delivery to other tissues.

Poloxamers, with the trade name Pluronic® (BASF, NJ, USA), are a family of more than 50 different amphiphilic nonionic block copolymers consisting of a central hydrophobic propylene oxide (PO) chain and two hydrophilic ethylene oxide (EO) polymer chains flanking both sides of the PO polymer. All poloxamers have similar structures, where PO and EO are arranged in EO_a-PO_b-EO_a structures and their hydrophilic-lipophilic balance is determined by the number of EO and PO moieties. Since their introduction, they have been used in a wide range of applications in the pharmaceutical and other biomedical industries as emulsifying, solubilizing, or dispersing agents and as in vivo absorbance enhancers [64]. Interestingly, poloxamers have been shown to promote drug penetration through the blood-brain barrier by inhibiting drug efflux transporters, suggesting that they would enhance drug biodistribution and allow targeting of viral reservoirs in the central nervous system [65]. Table 1 presents a list of select poloxamers and their respective properties. These poloxamers represent the best match to our needs as they can encase hydrophobic drugs by their PO hydrophobic central polymer chain while their EO hydrophilic polymer chains facilitate formation of an aqueous suspension.

Nanocrystals dispersed in aqueous suspension have demonstrated improvement in the clinical efficiency of drugs by 1) enhancing bioavailability; 2) lowering of dose requirement; and 3) facilitating sustained release of drugs. Having nanocrystals in

aqueous suspension has its own advantages: 1) drugs remain in the required crystalline state with reduced particle size, leading to increased dissolution rate, thus improved bioavailability; 2) drugs no longer need to be in soluble form, especially valuable for molecules insoluble in oils; 3) high drug loading can be achieved becaue drugs exist in the form of pure solid which can reduce the administration volume for high doses; and 4) nanosuspensions can increase the physical and chemical stability of drugs because they are in a solid state [66].

To prepare suspensions of nanosized crystals (nanosuspension), a high-pressure homogenization method was used. Advantages offered by this method are 1) even dispersion of ingredients within the medium; 2) good reproducibility; 3) an organic solvent-free method; 4) large-scale production capability by pharmaceutical industry because these homogenizers are available with different capacities ranging from hundreds to thousands of liters per day [67]. The formation of nanosuspensions with this method is based on the cavitation forces created in high-pressure homogenizers (Figure 2.1). After high-pressure homogenization, excessive poloxamer is removed by differential centrifugation to minimize the amount of excipient. However, this centrifugation process may result in particle aggregation during resuspension and limit large-scale manufacture.

Here we describe a simplified, scalable, and reproducible method for generating macrophage-targeted nanoparticles to abrogate purification process. The resultant nanoparticles demonstrated prolonged particle stability with good potential for large-scale manufacture.

Mean particle size, polydispersity index (PDI), and zeta-potential are important characteristic parameters to determine particle stability, dissolution rate, and in vivo behavior of nanosuspensions. Based on prior experience (Refs), particle size of 350 – 500 nm are most likely to form a stable formulation. The PDI is also an important parameter that governs the physical stability of nanosuspensions and should be as low as possible

for long-term stability of nanosuspensions. A PDI value of 0.1 – 0.3 indicates a fairly narrow size distribution, whereas PDI values greater than 0.5 indicate a very broad distribution [68]. Zeta-potential provides information about the surface charge of the particle and an impression about its long-term stability. The zeta-potential of a nanosuspension is governed by the stabilizer and the drug itself. For a nanosuspension stabilized by electrostatic repulsion, a minimum zeta-potential of ± 30 mV is required, whereas for a combined electrostatic and steric stabilizer, a zeta-potential of ± 20 mV would be sufficient [69].

2.3 Materials and Methods

2.3.1 Materials

ATV was purchased from Longshem Co. (Shanghai, China) and free-based with triethylamine. Poloxamers 407, 403, 338, 238, 237, and 188 were purchased from BASF (Florham Park, NJ). Dulbecco's Modified Eagle's Medium (DMEM) was purchased from Corning Life Sciences (Tewksbury, MA). Heat-inactivated pooled human serum was obtained from Innovative Biologics (Herndon, VA). Gentamicin, high performance liquid chromatograph (HPLC) grade acetonitrile (ACN), HPLC grade methanol, and Optima grade water were purchased from ThermoFisher Scientific (Waltham, MA, USA).

2.3.2 High-pressure homogenization

For preparation of nanosuspensions, 1% (w/v) ATV was added to a solution of 0.5% (w/v) poloxamer in 10 mM HEPES buffer, pH 7.8 (Figure 2.2). For optimized direct preparation, 1% (w/v) ATV was added to either 0.06% or 0.1% (w/v) poloxamer in 10 mM HEPES buffer, pH 7.8 (ATV to polymer ratio was 2:1). The premix was stirred with magnetic bar for 16 hours at room temperature followed by homogenization using high-pressure homogenizer (Avestin EmulsiFlex-C3; Avestin Inc., Ottawa, ON, Canada) at 20,000 psi until a desired particle size of 300-400 nm was attained.

2.3.3 Formulation purification by differential centrifugation

Crude nanosuspensions were purified by a series of centrifugations. The homogenized suspension was first centrifuged at 10,000 × g for 15 min. The supernatant was discarded, and the pellet was re-suspended in 0.2% (w/v) poloxamer solution. The re-dispersed nanoparticles were centrifuged at 200 × g for 1 min to remove large particles that were poorly dispersed. Supernatant from the secondary centrifugation was collected as the final formulation.

2.3.4 Nanoparticle physicochemical characterization

Nanoparticle diameter, PDI, and zeta-potential were measured by dynamic light scattering (DLS) using a Malvern Zetasizer, Nano Series Nano-ZS (Malvern Instruments, Inc, MA, USA). All measurements were performed with samples stored at 25 °C without stirring. Encapsulation efficiency for the formulation was calculated by the following equation:

$$\text{Encapsulation efficiency (\%)} = \frac{weight\ of\ drug\ in\ formulation}{weight\ of\ drug\ added} \text{ X } 100$$

2.3.5 Nanoparticle monocyte-derived macrophage uptake

Human peripheral blood monocytes were obtained and cultured as described previously [70]. Briefly, peripheral blood monocytes were obtained by leukapheresis from HIV-1/2 and hepatitis B seronegative donors, followed by purification by countercurrent centrifugal elutriation. Monocytes were cultured in DMEM supplemented with 10% heat-inactivated pooled human serum, 10 µg/mL ciprofloxacin, 50 µg/mL gentamicin, and 1,000 U/mL recombinant macrophage colony stimulating factor to drive monocyte-macrophage differentiation. Monocytes were allowed to differentiate to macrophages for 7-10 days. Then cells were treated with 100 µM ATV nanoformulations. At predetermined time points, MDMs were washed three times with sterile phosphate-buffered saline (PBS) and scraped

into 1 mL PBS. Cell pellets were collected by centrifugation at 2,000 × g for 8 min, followed by probe sonication in 200 µL HPLC grade methanol to extract ATV.

2.3.6 ATV quantitation

ATV concentration was measured by HPLC. We assessed the samples by reverse phase HPLC using triplicate 10 µL injections onto a YMC Octyl C8 column (Waters Inc, Milford, MA). Mobile phase consisting of 48% ACN / 52% 25 mM KH_2PO_4, pH 4.15 at flow rate of 0.4 mL/min with UV/Vis detection at 272 nm. Quantification was determined by comparison of peak areas to a standard curve of ATV (0.05-50 µg/mL) in methanol.

2.4 Results

2.4.1 ATV nanoformulation (NATV) synthesis with purification

NATV was prepared by premixing ATV with different poloxamers illustrated in Table 2.1 (P407, 403, 338, 238, 237, or 188) with drug to polymer weight-to-weight ratio 2:1. After overnight mixing, the premixes were processed by high-pressure homogenization to reduce the particle size. The size and PDI of the nanoparticles produced with different poloxamers were comparable as follows 350-450 nm and 0.25-0.3, respectively. However, the zeta-potential was variable ranging from -5 to -20 mV. Nevertheless, after differential centrifugation, approximately 30% of the drug was lost and encapsulation efficiency reduced to 70% during this process. Additionally, only 3 formulations retained particle sizes of 400-500 nm (ATV-P407, ATV-P403, and ATV-P338) whereas all other formulations were aggregated, reaching particle sizes of several microns. Of those that maintained the desired particle size, only ATV-P403 remained within the acceptable range while the others all aggregated by day 7 (Figure 2.3A). These results were concomitant with PDI measurements (Figure 2.3B). Surprisingly, zeta-potential of the three nanoformulations did not change until day 7 (Figure 2.3C).

2.4.2 ATV nanoformulation by direct manufacture

To preclude particle aggregation caused by harsh pressure during differential centrifugation, we determined the polymer content required to develop a simplified direct manufacture method to avoid centrifugation (Figure 2.4). To achieve this, the drug to polymer ratios were determined by evaluation of integral areas in the proton nuclear magnetic resonance (^{1}H-NMR) spectra as described previously [71]. To optimize manufacture conditions, two drug-to-polymer ratios were tested, 100:10 and 100:6. NATV prepared by direct manufacture at either drug-to-polymer ratio exhibited high drug loading without compromising particle integrity. High-pressure homogenization achieved stable nanoparticles in terms of particle size and PDI with all tested poloxamers for at least 8 weeks except for ATV-P338 100:6 and ATV-P188 100:6 that did not remain stable beyond 3 and 1 week, respectively (Figure 2.5A and B). However; the zeta-potential of all formulations remained within the acceptable range for 8 weeks (Figure 2.5C).

2.4.3 NATV uptake and retention in MDMs

The elimination of the purification step after homogenization significantly enhanced particle stability and increased encapsulation efficiency to more than 90%. Therefore, nanoformulation prepared by direct manufacture was moved to MDM uptake and retention studies. Since ATV made stable nanoparticles with all tested poloxamers at a 100:10 drug-to-polymer ratio, these formulations were tested for MDM uptake and retention. Treatment of MDMs to NATV showed increasing drug uptake for the course of 8 hours. Although ATV-P407 and -P188 exhibited the highest uptakes, there were no significant differences in uptake among all tested poloxamers (Figure 2.6A). After 8-hour exposure of MDMs to NATV, the drug was retained intracellularly for at least 15 days, with no significant differences among the tested poloxamers (Figure 2.6B).

2.5 Discussion

LA ARVs show promise providing prolonged dosing intervals and less fluctuation in plasma drug levels, presumably improving therapeutic outcomes for HIV/AIDS. LA ARVs have potential to improve regimen adherence, reduce systemic toxicities antiviral mutations, and reduce the stigma related to daily regimens of ART [58, 72]. A successful regimen requires high drug encapsulation that would maintain a sufficient amount of drug for months and with a readily injectable volume. In addition, loaded drugs toned to be released in a pattern that is sufficient to provide therapeutic drug levels, yet slow enough to avoid high concentrations with their related toxicities and to achieve prolonged dosing intervals.

Nanocrystals provide an improved strategy to formulate hydrophobic LA ART. They offer high drug loading capacity while eliminating organic solvent usage, therefore reducing relevant toxicities. After injection of the nanocrystals, the injection site serves as a primary depot from which drug is dissolved and eventually released into the circulation. Sustainable release for weeks to months can be achieved with drugs that have low aqueous solubility. RPV and CAB LA formulations are both nanocrystals with approximately 200 nm diameters manufactured by wet-milling, a commonly used top-down method to prepare nanoparticles. The presence of surfactants such as polysorbates and poloxamers is essential to prevent particle aggregation. High-pressure homogenization is another size reduction technique that reduces particle size by forcing of a suspension under pressure through a valve with a narrow aperture [73]. This method presumably precludes formulation contamination from the worn beads that are used in wet-milling.

Poloxamers are widely used surfactants in the pharmaceutical industry because of their unique characteristics. Having both hydrophilic and lipophilic polymer chains, they

have been used to formulate poorly water-soluble drugs, in addition to their capabilities to make LA suspensions. Although each poloxamer has unique physiochemical characteristics, particularly hydrophilic-lipophilic balance, all tested poloxamers resulted in stable formulations after direct manufacture, except for ATV-P338 and -P188 with a 100:6 drug-to-polymer ratio. Failure of these formulations can likely be attributed to a low amount of poloxamer that was presumably insufficient to fully encase the drug.

Macrophages and CD4^{+} T cells are primary cellular reservoirs for HIV-1 [30]. Our next goal is to employ macrophages as "Trojan horses" to deliver nanoparticle drugs to another cellular target. Macrophages are highly mobile cells and readily cross biological barriers to sites of inflammation and infection. Drug crystals in the endosomal compartments of macrophages could therefore cross physiological barriers to reach viral reservoirs such as the gut, brain, and lymph node [31]. Depending on surface chemistry and lipophilic properties, nanoparticles phagocytosed by macrophages can be released into the blood stream and surrounding tissues. This secondary depot should further reduce maximal plasma drug concentration (Cmax) and prolong apparent half-life (t1/2), which could potentially reduce overall dosage as well as drug-induced toxicities.

seems out of place here

2.6 Conclusions

Though current LA ART nanoformulations demonstrate real potential for improving HIV management and prevention, further refinements in medicinal and polymer chemistry, for example increasing lipophilicity of the drug, could produce a more optimal drug delivery system and further improve viral restriction [50, 74].This study focused on overcoming the technical hurdles that are commonly faced during nanoformulation preparation. The direct manufacture procedure used here is highly reproducible and scalable and could be

applied to other similar formulation platforms, which represents an important step forward in development and translation of next generation LA ART.

2.7 Figures and tables
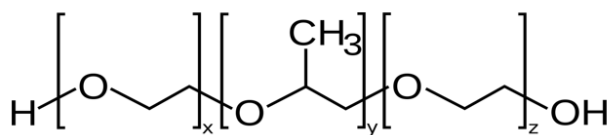
Name	Trade Name	Value of x	Value of y	Value of z	HLB
P-407	Pluronic F-127	98	67	98	22
P-403	Pluronic P-123	21	67	21	8
P-338	Pluronic F-108	128	54	128	27
P-238	Pluronic F-88	97	39	97	28
P-237	Pluronic F-87	62	39	62	24
P-188	Pluronic F-68	153	29	153	29

Table 2.1 Poloxamer characteristics. The table shows select poloxamers and their composition along with their hydrophilic-lipophilic balance (HLB). A higher y value renders the poloxamer more lipophilic whereas higher x or z values makes it more hydrophilic.
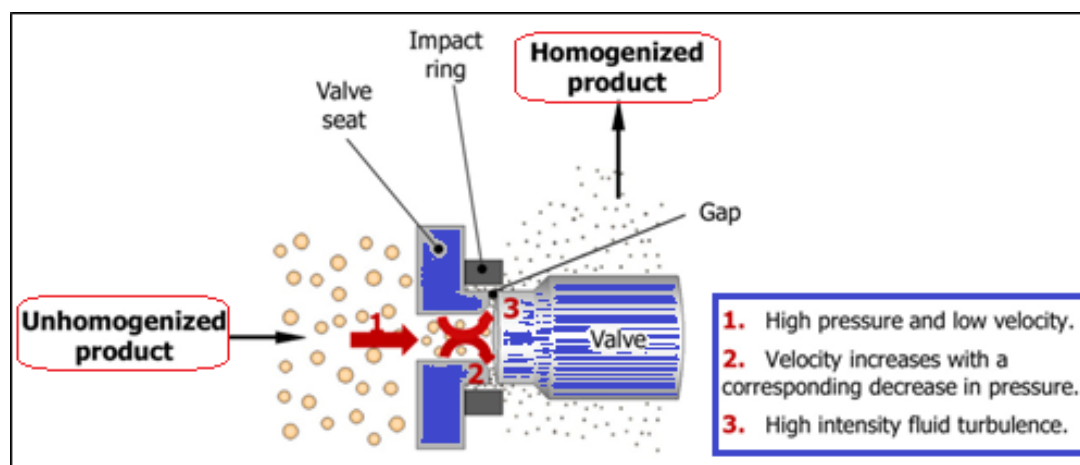
Figure 2.1 High-pressure homogenization. The pre-suspension passes through a very small homogenization gap in the homogenizer, typically having a width of 25 µm at 1500 bar. Due to the narrowness of the gap, the streaming velocity of the suspension and the dynamic fluid pressure increases. In addition, the static pressure on the fluid decreases below the boiling point of water at room temperature. Consequently, water starts boiling at room temperature and gas bubbles are formed that implode (cavitation) when the fluid leaves the homogenization gap. These cavitation forces are strong enough to break the drug microcrystals into nanocrystals.

The figure was modified from [73].
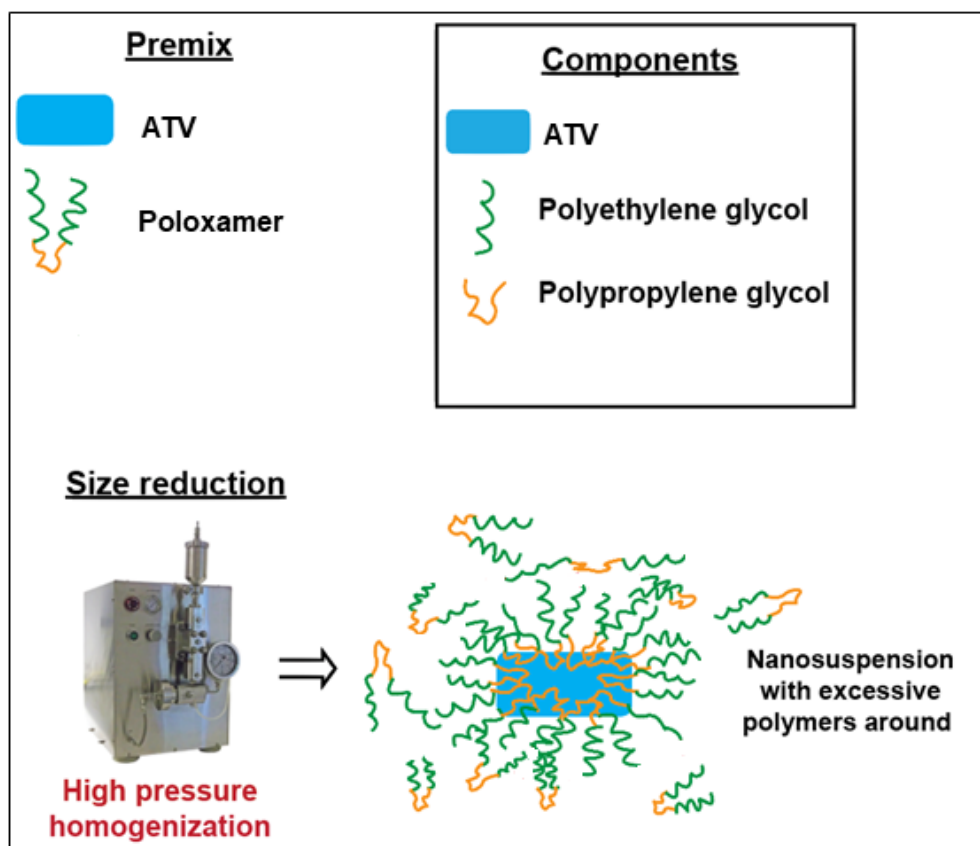
Figure 2.2 Particle size reduction scheme. ATV was dispersed with the poloxamer followed by high-pressure homogenization until the desired particle size and PDI were achieved. The resultant nanosuspension contains excessive polymer that requires purification.
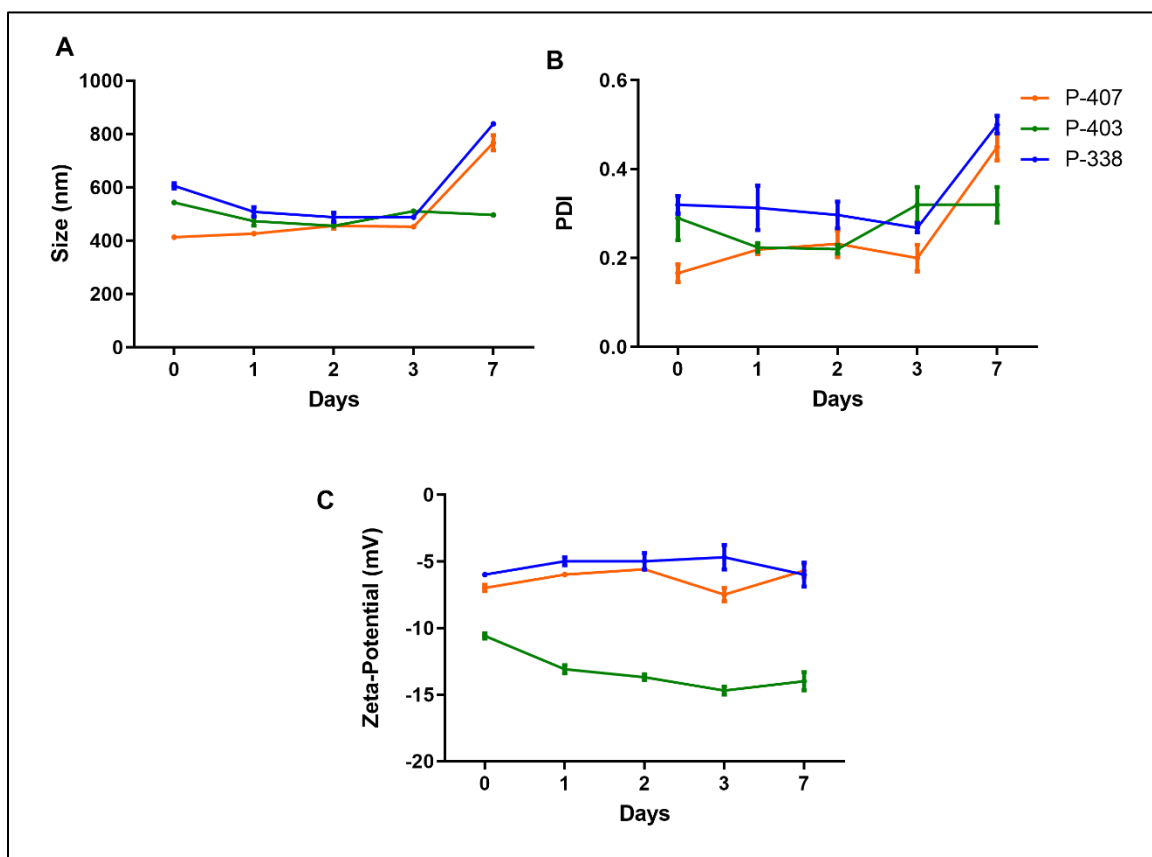
Figure 2.3 NATV stability after purification. Only 3 nanoformulations had stable particle size (A)and PDI (B) for 3 days after the purification step; ATV-P407 and -P338 aggregated by day 7. The zeta-potential (C) did not change during the course of the study with any of the nanoformulations.
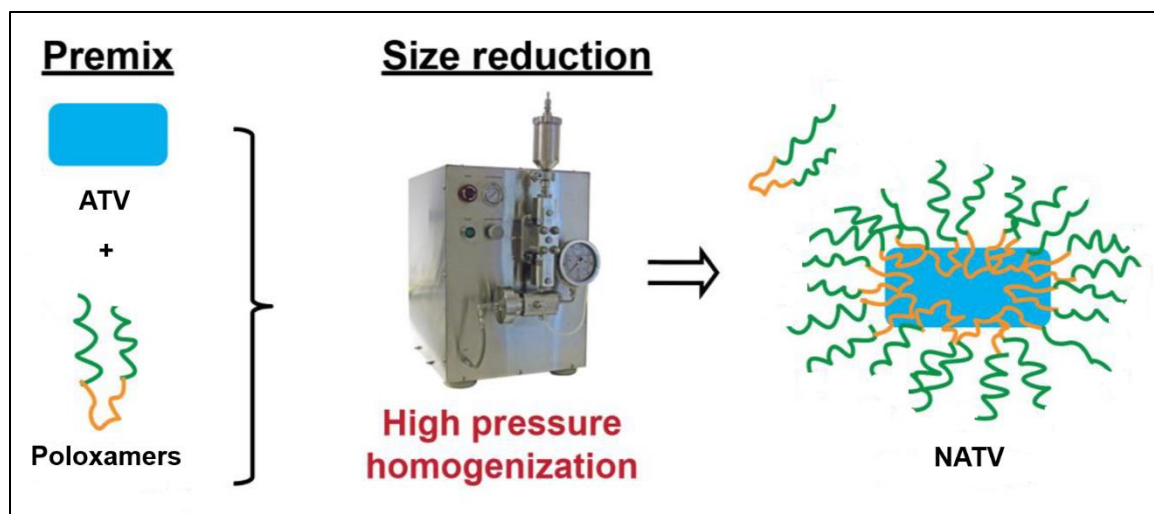
Figure 2.4 NATV Direct manufacture. Direct manufacture process where drug to polymer ratio was optimized to preclude the need for removal of excessive polymer by centrifugation.
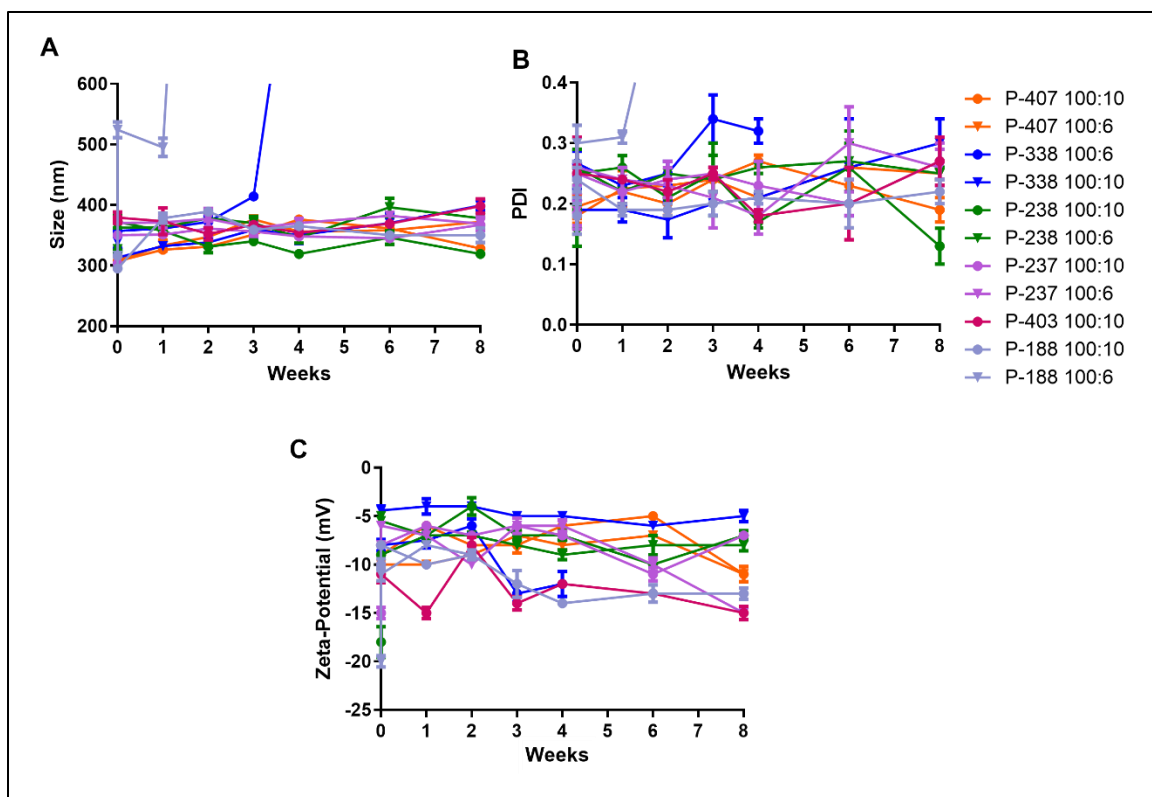
Figure 2.5 NATV stability after direct manufacture. Avoiding centrifugation after homogenization resulted in stable nanoparticles in terms of (A) particle size and (B) PDI for 8 weeks except for ATV-P338 and -P188 at 100:6 drug-to-polymer ratio. (C) the zeta-potential remained within an acceptable range for 8 weeks.
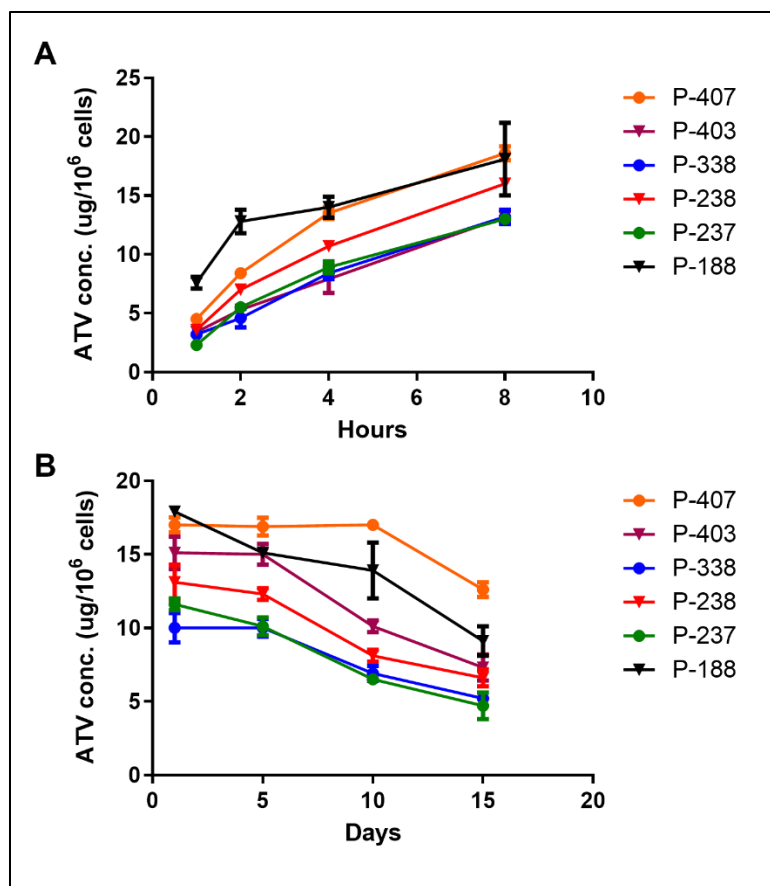
Figure 2.6 NATV uptake and retention in MDMs. (A) Exposure of MDMs to NATV resulted in steady increasing uptake. (B) After 8-hour exposure, the drug was retained in MDMs for at least 15 days. No significant differences were found among all tested poloxamers.

Chapter III. Synthesis and Characterization of a Long-Acting Emtricitabine Prodrug Formulation

3.1 Abstract

Aims: A palmitoylated prodrug of FTC was synthesized then encased into a LA nanoformulation extending the native drug's apparent half-life, antiretroviral activities, and biodistribution to tissue viral reservoirs.

Methods: A chemically modified FTC prodrug (MFTC) was synthesized by esterification with palmitoyl chloride. MFTC's structure and crystallinity were confirmed by ^{1}H- and ^{13}C-NMR, Fourier transform infrared spectroscopy and X-ray diffraction. A P407 coated aqueous nanosuspension of MFTC (NMFTC) was prepared by high-pressure homogenization. NMFTC uptake, retention and antiretroviral efficacy were examined in human MDMs. Drug PK and tissue distribution were evaluated in Sprague-Dawley rats after a single IM injection of 45, 75, or 100 mg/kg FTC-equivalents. FTC and its active triphosphate metabolite (FTC-TP) were quantified by liquid chromatography tandem mass spectrometry.

Results: FTC was conjugated to the long chain fatty acid palmitoyl chloride. The hydrophobic prodrug coated with P407 formed stable water insoluble nanocrystals. NMFTC exhibited particle sizes of 350 ± 30 nm, PDI of 0.24 ± 0.02, zeta potential of -20 ± 2 mV, and encapsulation efficiency of 85%. MFTC nanoparticles were readily taken up by MDMs with high intracellular FTC-TP and extended PK profiles.

Conclusion: LA NMFTC showed physicochemical stability, improved antiretroviral efficacy and extended plasma half-life compared to its native drug. This work represents a step forward in the development of LA FTC drug therapies.

3.2 Introduction

UNAIDS has recently highlighted the significant toll seen by HIV infections worldwide [12]. In 2017, approximately 37 million people worldwide were infected. Of those, 1.8 million were children under the age of 15. Despite global efforts to treat and

prevent viral infection, about 1 million people have died of the infection. Equally concerning is that only 21.7 million infected people had access to ART. It is estimated that $26.2 billion will be required to control and prevent HIV infection in the developing world by 2020.

To reduce the spread of HIV infection, improved access to ART and continuous adherence to therapeutic regimens are needed. Effective treatment of infection requires early, daily, and lifelong therapy [75]. While currently available therapeutic regimens have demonstrated remarkable success in reducing disease morbidity and mortality, treatment failures abound. These are due, in part, to patient non-adherence to complex drug regimens and to the stigma of infection itself [76, 77]. Nonetheless, cART regimens are required to ensure reductions in viral load, maintenance of CD4+ T cell counts, prevention for the emergence of drug resistant viral strains, and in eliminating viral transmission [78]. The inability of current antiretroviral drugs (ARVs) to target viral reservoirs (including the lymph nodes, gut, central nervous system, genitourinary system and spleen) has also reduced therapeutic success [79].

To address each and more of these limitations, LA ARV regimens were developed. They serve to improve patient adherence, decrease drug toxicities, and maintain viral suppression while also diminishing the stigma of ARV use. LA ART are made by encasing ARVs into poloxamer coated nanocrystals that facilitate intracellular drug depots at the injection site and within macrophages of the reticuloendothelial system and other tissue viral compartmentalization sites [80]. At present, LA ART are highly protein bound, metabolized and released slowly, and housed in depots where drug is released in time measured from days to weeks. Research in our own laboratories have extended this drug platform by the use of MDMs as cell-based drug depots and as vehicles for drug delivery to viral reservoir tissue sites [81]. Each of these serve to improve ARV PK and pharmacodynamics (PD) profiles [82].

Despite active research into LA ARVs only two antiretrovirals, CAB and RPV are now being developed for human use as LA medicines [59]. Thus, there is an imperative for further research and drug development in this area. This is especially important for LA transformation of the NRTIs as they represent the backbone of current ART regimens. Indeed, the standard of care once a day antiretrovirals are administered as two NRTIs and an integrase or NNRTI [83]. Amongst these, the most potent and widely used NRTIs for treatment of infection are FTC, TDF and 3TC [84-86]. Truvada®, a once daily regimen of FTC and TDF, combination has also shown to be effective in PrEP [54]. Thus, expanding available LA formulations for each or all of these medicines would have a significant impact on the care, treatment and prevention of HIV/AIDS.

In efforts to achieve a once-a-month or even longer dosing frequencies, our laboratory has recently created LA NRTI prodrug formulations [48, 51]. While a dream a few years ago, creating a LA ARV library is now within reach [49, 51, 52, 87, 88]. Notably and in the present report, FTC was chemically modified to create a LA agent. FTC was chosen based on its bioavailability and limited toxicity profiles [53]. FTC is a potent cytidine analogue that is transformed into its active triphosphate metabolite in cells where it competes with endogenous cytidine triphosphates for incorporation into the viral DNA chain during viral reverse transcription [89]. A major obstacle in transforming FTC into a LA agents rested in its hydrophilicity. With this in mind we created a first-generation hydrophobic FTC prodrug amenable to nanoparticle encasements. This was done by conjugating it to a long chain palmitoyl fatty acid. The hydrophobic nanocrystal prodrugs were stabilized into an aqueous solution by P407. The nanosuspension offered increased dissolution rates and long term profiles as drugs remain in nanocrystals with high encapsulation efficiency, and physicochemical stability [45]. The developed nanoparticles are readily taken up by MDMs and reside inside subcellular endosomes for prolonged time

period with stable FTC-TP conversion levels. PK profile assessed in rats was significantly improved over the native drug. As such, this nanoformulated FTC prodrug could be employed as a first step in formulation development with the aim of improving patient adherence, reducing adverse reactions and targeting drug to HIV infectious reservoirs.

3.3 Materials and methods

3.3.1 Materials

FTC was purchased from HBCChem (Union City, CA). Palmitoyl chloride, tetrahydrofuran (THF), tert-butylmagnesium chloride (tBuMgCl), 4-(2-hydroxyethyl)-1-piperazineethanesulfonic acid (HEPES) buffer, ciprofloxacin, dimethyl sulfoxide (DMSO), paraformaldehyde (PFA), ammonium acetate, 3,3`-diaminobenzidine (DAB), type XA acid phosphatase (EC 3.1.3.2) from sweet potatoes, Histopaque-1083, and Hank's Balanced salt solution (HBSS) were purchased from Sigma Aldrich (St. Louis, MO). Poloxamers 407, 403, 338, 238, 237, and 188 were purchased from BASF (Florham Park, NJ). Thin-layer chromatography was performed on precoated F-254 silica plates (250 µm) from SiliCycle, Inc. (Quebec City, QC, Canada). LC-MS grade water, PBS, diethyl ether, gentamycin, ACN, methanol, Triton X-100, and dichloromethane (DCM), acetic acid, and ammonium hydroxide were purchased from Fisher Scientific (Waltham, MA). DMEM was purchased from Corning Life Sciences (Tewksbury, MA). Monoclonal mouse anti-human HIV-1 p24 (clone Kal-1), monoclonal mouse anti-human leukocyte antigen (HLA-DP/DQ/DR; clone CR3/43), and the polymer-based HRP-conjugated anti-mouse EnVision+ secondary antibody were purchased from Dako (Carpinteria, CA). cell counting kit-8 (CCK-8) was purchased from Dojindo Molecular Technologies, Inc. (Rockville, MD). FTC-TP was purchased from Toronto Research Chemicals (North York, Canada). Sep-Pak QMA anion-exchange cartridges and OASIS HLB reverse-phase cartridges were

purchased from Waters Corp. (Milford, MA). Potassium chloride (KCl) was purchased from JT Bakers Co. (Phillipsburg, NJ).

3.3.2 MFTC synthesis and characterization

FTC (2.0 g, 8.089 mmol, 1 equivalent) was dried by azeotroping from anhydrous pyridine (15 mL), resuspended in anhydrous THF (30 mL), cooled to -78°C, followed by addition of ^{t}BuMgCl (8.089 mmol, 1 equivalent, 1 M in THF) and allowed to stir for 15 minutes under an argon atmosphere. A solution of palmitoyl chloride (2.26 g, 8.089 mmol, 1 equivalent) was then added dropwise to the FTC anion at -78°C. The reaction mixture was gradually warmed to room temperature and stirred for 16h, quenched using saturated ammonium chloride solution, concentrated, and subjected to flush chromatography purification to isolate MFTC as a colorless powder. Proton (^{1}H)- and carbon (^{13}C)- NMR spectra were recorded on a Varian Unity/Inova-500 NB (500 MHz; Varian Medical Systems Inc., Palo Alto, CA). FTIR was performed on a PerkinElmer universal attenuated total reflectance (UATR) Spectrum Two (Waltham, MA). The aqueous solubility of FTC and MFTC were determined by adding excess drug to water followed by mixing for 24 h at room temperature. Samples were centrifuged at 14,000 rpm for 10 min to remove undissolved drug. Solubilized drug in the supernatant was quantified using a Waters ACQUITY ultra-performance liquid chromatography (UPLC) with TUV detector and Empower 3 software (Milford, MA). FTC and MFTC drug extracts were separated on a Phenomenex Kinetex 5 µm C18 column 100A (Torrance, CA) using either 95% 20 mM ammonium acetate buffer in 5% ACN, pH 3.9, or 90% methanol/10% water with a flow rate of 1.0 mL/min and detected at 272 and 280 nm, respectively. Drug content was quantified by comparison of peak areas of known standards (0.05-50 µg/mL).

3.3.3 Nanoformulation preparation and characterization

For preparation of NMFTC nanosuspension, a pre-suspension of 1% (w/v) MFTC and 0.5% (w/v) P407 in 10 mM HEPES buffer (pH 5.5) was made and nanosized by high-pressure homogenization (Avastin EmulsiFlexC3; Avastin Inc., ON, Canada) at 20,000 psi until the desired particle size of 300-400 nm was achieved. Particle size, PDI, and zeta-potential were assessed by DLS using a Malvern Zetasizer Nano Series Nano-ZS (Westborough, MA). The stability of NMFTC was monitored at room temperature and 4 °C for up to 10 weeks in terms of particle size, PDI, and zeta-potential. The crystalline structures of MFTC was determined by X-ray diffraction (XRD) that was performed in the 2θ range of 2–40° using a PANalytical Empyrean diffractometer (Westborough, MA) with Cu-Kα radiation (1.5418 Å) at 40 kV and 45 mA setting. A mask of 20 mm and a divergence slit of 1/8° were used on the incident beam path. The diffraction data was collected in steps of 0.04 degrees by continuously scanning at the rate of 0.013 °/s.

3.3.4 Nanoparticle macrophage uptake, retention, and cytotoxicity

Human peripheral blood monocytes were obtained from HIV- and hepatitis-seronegative donors and purified by centrifugal elutriation at the University of Nebraska Medical Center (UNMC) elutriation core facility. The monocytes were cultured on 12-well plates at a density of 1 million cells per well and allowed to differentiate into macrophages in DMEM culture media consisting of 10% human serum, 1% glutamine, 50 μg/mL gentamicin, 10 μg/mL ciprofloxacin, and 1000 U/mL macrophage colony-stimulating factor for 7–10 days. Cell uptake was assessed at various time points after incubation with 100 μM NMFTC. At each time point, adherent MDMs were washed three times with 1 mL PBS, scraped into 1 mL PBS, and pelleted by centrifugation at 8,000 rpm for 8 minutes at 4 °C. The cell pellet was reconstituted in 200 μl of methanol and probe-sonicated at 15% amplitude (QSonica Q55; Qsonica, LLC, CT, USA), followed by centrifugation at 14,000 rpm for 10 minutes at 4 °C to pellet cell debris. FTC or MFTC concentration in the

supernatant fluid was quantified by UPLC as described above. To determine the extent and duration of retention, cells were incubated with 100 μM NMFTC for 8 hours and then washed with PBS to replace the medium with fresh drug-free medium. At various time points, cells were washed with PBS, collected, and analyzed for drug concentrations as described for the uptake study. For cellular cytotoxicity assay, monocytes were cultured on a 96-well plate at a density of 8,000 cells per well and allowed to differentiate into macrophages as described above. MDMs were exposed to various concentrations of the drug ranging from 0.05 – 500 μM. After 24 h, 10 μL of CCK-8 solution was added to each well, followed by 2 h incubation prior to absorbance measurement at 450 nm wavelength on a Molecular Devices SpectraMax M3 plate reader with SoftMax Pro 6.2 software (Sunnyvale, CA).

3.3.5 NMFTC antiretroviral activities

Antiretroviral efficacy was determined by measuring HIV RT activity. For half maximum effective concentration (EC_{50}) determination, MDMs were exposed to various concentrations (0.01-1000 nM) of MFTC for 1 h followed by challenge with HIV-1$_{ADA}$, a monocyte-tropic variant of HIV-1, at a multiplicity of infection (MOI) of 0.1 infectious particles per cell for 4 h. After viral challenge, cells were washed and incubated with the same concentration of drug used before infection for an additional 10 days. Culture fluids were collected on day 10 for measurement of RT activity as previously described [90, 91]. To evaluate the antiretroviral efficacy, MDMs were exposed to 100 μM NMFTC for 8 hours. The cells were then washed with PBS to remove any remaining nanoparticles not taken up by the cells. At various time points, the MDMs were then challenged with HIV-1$_{ADA}$, at a MOI of 0.1 infectious viral particles per cell for 18 hours. Ten days after each challenge, viral activity was determined by measuring RT activity in the culture medium as previously described [90, 91]. HIV-1 p24 antigen expression was assessed on adherent cells as follows. After collecting the medium for RT assay, cells were washed with PBS and then

fixed with 4% PFA for 15 min at 37 ℃. Non-specific antibody binding on the cell surface was blocked using 10% bovine serum albumin containing 1% Triton X-100 in PBS for 30 min at room temperature. Following blocking, cells were incubated with HIV-1 p24 mouse monoclonal antibodies overnight at 4 °C, followed by 1-hour incubation at room temperature. HRP-conjugated polymeric anti-mouse secondary antibody was added as one drop per well. Hematoxylin was added to counterstain the nuclei and images were visualized from a Nikon TE300 microscope with a 20X objective.

3.3.6 Particle morphology: transmission electron microscopy (TEM)

TEM was used to visualize the morphology of the nanoparticles, and to visualize nanoparticles taken up by macrophages. For nanoparticle morphology, the nanosuspension was dried on a copper grid at room temperature and bright field images were taken with exposure times of 2 s. Macrophages loaded with nanoparticles were analyzed after NMFTC exposure for 4 h. Cells were collected in PBS, centrifuged at 3000 rpm for 8 min at room temperature. The cell pellet was fixed in a solution consisting of 2% glutaraldehyde, 2% PFA in 0.1 M Sorenson's phosphate buffer (pH 6.2). During processing, samples were post-fixed in a 1% aqueous solution of osmium tetroxide for 30 minutes. Subsequently, samples were dehydrated in a graded ethanol and propylene oxide used as a transition solvent between the ethanol and araldite resin. Samples were allowed to sit overnight in a 50:50 propylene oxide:resin solution until all the propylene oxide had evaporated then they were incubated in fresh resin for 2 h at room temperature before embedding. Polymerization took place at 65°C for 24 h. The staining procedure was 10 minutes in 2% (w/v) uranyl acetate, washed 3 times in distilled water, 10 minutes in Reynolds Lead Citrate, and washed 3 times in distilled water. Thin sections (100 nm) made with Leica UC6 Ultracut ultramicrotome were placed on 200 mesh copper grids. Both copper grids, for nanoparticles and macrophages, were examined on FEI Tecnai G2

Spirit TWIN electron microscope (Hillsboro, OR) operating at 80kV. Images were acquired digitally with AMT imaging system (Woburn, MA).

3.3.7 MFTC plasma stability

To determine differences in MFTC plasma stability across species, 100 µL of mouse, rat, rabbit, dog, monkey, and human plasma were incubated with 1 µM MFTC at 37 °C. At 0, 30, and 90 min, 1 mL methanol was added to each sample and vortexed for 3 min to stop the reaction. For the 0-min time point, 100 µL ice cold plasma was spiked with 100-x prodrug spiking solution in 20% DMSO/80% methanol and immediately after, 1 ml of ice-cold methanol was added. Heat-inactivated plasma was incubated under the same conditions and used as a negative control to differentiate chemical vs. biological instability. Following the addition of methanol, samples were centrifuged at 15,000 x g for 10 min, 10 µl of supernatant was mixed with 80% methanol containing IS, and then 10 µl was used for liquid chromatography-tandem mass spectrometry (LC-MS/MS) analysis. MFTC and FTC concentrations were determined in the supernates by UPLC-MS/MS.

3.3.8 Pharmacokinetics

Male Sprague-Dawley rats (Charles River Laboratories, Wilmington, MA) maintained on normal diet were injected IM with FTC or NMFTC at a dose of 45, 75, or 100 mg/kg FTC-equivalents in the caudal thigh muscle. Blood was collected at 2 hours, and days 1, 7, and 14; and tissues, including liver, spleen, lymph nodes, and brain, were collected at days 1, 7 and 14. FTC was quantified by LC-MS/MS with modification of an established method [92]. Briefly, 25 µL of plasma samples and a 100 µL of tissue homogenates in 90% methanol were spiked with internal standard ($^{15}N_2$$^{13}C$- lamivudine at 80 ng/ml, final concentration of 8 ng/ml), and extracted with methanol-protein precipitation. Plasma and tissue standards were prepared at final concentrations in the range of 0.05-

500 ng/ml. FTC was quantified by a LC-MS/MS system consisting of a Waters ACQUITY H class liquid chromatography system coupled to a Waters Xevo TQ-S micro mass spectrometer (Waters Corp., Milford, MA, USA) with an ESI source in positive mode. An ACQUITY UPLC® CSH C18 1.7 μm analytical column (2.1mm×100mm, Waters Corp.) with an ACQUITY CSH C18 Vanguard column (2.1mm×5mm, Waters Corp.) were used for analyte separation. The transition of 247.98 < 129.80 m/z and 233.23 < 114.97 m/z were used for FTC and IS quantification. Mobile phase A consisted of 7.5 mM ammonium bicarbonate in water (MS grade, Fisher), pH was adjusted to 7.0 with glacial acetic acid (ACS grade, Sigma). Mobile phase B was 100% methanol (MS grade, Fisher). The flow rate was 0.25 mL/min.

3.3.9 Cell isolation for FTC-TP extraction

On each sacrifice day, cells from fresh blood, spleen, and lymph nodes were isolated and stored in 70% methanol as previously described [92]. PBMCs from rat blood were isolated using Histopaque-1083 according to the manufacturer's protocol. Briefly, blood collected in EDTA tubes was layered on top of 1 mL Histopaque-1083 and centrifuged for 30 min at 400 x g at room temperature. PBMCs were then aspirated, washed twice with PBS, resuspended in 0.2 mL PBS, and cell number was counted. Spleens were cut into small pieces and transferred onto 70 μm nylon cell strainers. Spleens were minced using the rubber end of the 3-mL syringe plunger, and cells were pushed through the cell strainer with HBSS. Cell suspensions were centrifuged at 200 x g for 10 min, and supernatants were discarded. Red blood cells were lysed by resuspending the pellet in 1 mL of ACK lysing buffer, followed by incubation for two minutes at 37 °C. Samples were neutralized with 10 mL HBSS, centrifuged at 200 x g for 10 min for washing twice. For lymph node lymphocyte isolation, rat lymph nodes were collected at each time-point, and cells were isolated as described for splenocytes, except that lymphocytes did not require red blood cell lysis. Both splenocytes and lymphocytes were eventually

resuspended in 1 mL PBS and cell numbers were carefully counted. Finally, all cells were centrifuged at 400 x g for 10 min and cell pellets were lysed with 200 µl of cold 70% Methanol and stored in -80 °C for later TP extraction. All cell counting was performed using Invitrogen Countess Automated Cell Counter (Carlsbad, CA).

3.3.10 FTC-TP quantification

FTC-TP extraction was performed as described previously [92]. Sep-Pak QMA cartridges (360 mg, 37–55 µm) were used to separate FTC-TP from its mono- and di-phosphate forms. The QMA cartridges were conditioned with 10 mL of 500 mM KCl followed by 10 mL of 5 mM KCl. Cell samples in 200 µl of 70% Methanol were loaded onto the cartridges and washed with 14 mL of 75 mM KCl. The triphosphate fractions were eluted with 3 mL of 500 mM KCl. The pH of the TP fractions was lowered by adding 45 µl ammonium acetate buffer (pH 4, 10 mM), and dephosphorylated by adding 3 µl type XA sweet potato acid phosphatase. The reaction was allowed to proceed in 37 °C shaking incubator for up to 1 hour. The $^{15}N_2^{13}C$-3TC internal standard was added following the incubation (10 µl of 5 ng/mL, final concentration of 0.5 ng/mL). Following preconditioning with 3 mL Methanol and 3 mL H_2O, samples were loaded onto Waters OASIS HLB cartridges (60 mg, 30 µm), then washed with 3.5 mL H_2O to remove KCl. FTC was then eluted with 1.4 mL of Methanol and evaporated under vacuum. Once dry, the residues were stored at −20 °C then reconstituted with 100 µl 25% methanol before performing LC–MS/MS analyses as mentioned earlier

3.3.11 Statistics and data analyses

All data are presented as mean ± standard deviation (SD) or standard error of the mean (SEM) for *in vitro* and *in vivo* studies, respectively. *In vitro* studies were performed using a minimum of three biological replicates. *In vivo* studies included a minimum of 3 animals per treatment group. For comparisons of two groups, Student's t test (two-tailed)

was used. For comparison between multiple groups, one-way ANOVA with Bonferroni correction were performed. For studies with multiple time points, two-way ANOVA and Bonferroni's post hoc tests for multiple comparisons were performed. Results with $P <$ 0.05 were considered significant. All data were graphed and analyzed using GraphPad Prism 6.0 software (La Jolla, CA).

3.3.12 Study approvals

All experimental protocols involving the use of laboratory animals were approved by the UNMC Institutional Animal Care and Use Committee ensuring the ethical care and use of laboratory animals in experimental research. All animal studies were performed in compliance with UNMC institutional policies and NIH guidelines for laboratory animal housing and care. Human blood cells were isolated by leukapheresis from HIV-1/2 and hepatitis seronegative donors and were deemed exempt from approval by the Institutional Review Board of UNMC.

3.4 Results

3.4.1 MFTC chemical analyses

To overcome challenges associated with the short half-life of hydrophilic water-soluble FTC, we created poloxamer-encased hydrophobic drug nanosuspensions with enhanced cellular drug uptake and improved antiretroviral efficacy [93]. To perform this task a 16-carbon fatty acid palmitoyl chloride was conjugated to FTC to form a hydrophobic ester prodrug, MFTC, with a final yield of 90% (Figure 3.1). The chemical modifications of FTC were confirmed by (^{1}H) and carbon (^{13}C) NMR spectra (Figure 3.2A and B, respectively), and FTIR spectroscopy. ^{1}H-NMR spectrum showed peaks corresponding to terminal methyl group (CH_3R) and repeating methylene (RCH_2R) protons of the fatty acid chain. ^{1}H NMR (500 MHz, $CDCl_3$): 7.94 (d, J = 6.5 Hz 1H), 6.27-6.31 (m, 1H), 5.35 (q, J = 4.3 Hz 1H), 4.43 (dd, J = 12.5, 2.9 Hz, 1H), 3.56 (dd, J = 12.4, 5.3 Hz, 1H), 3.18 (dd, J = 12.4,

3.1 Hz, 1H), 2.40 (t, $J = 7.5$ Hz 1H), 1.63-1.70 (m, 4H), 1.25 (br, 24H), 0.87 (t, $J = 6.9$ Hz 1H). ^{13}C NMR (125 MHz, CDCl$_3$): δ 173.1, 157.9, 157.8, 153.5, 137.1, 135.2, 125.8, 125.6, 87.4, 84.6, 63.2, 38.9, 34.0, 31.9, 29.8, 29.7, 29.6, 29.4, 29.3, 29.2, 29.1, 24.8, 22.7, 14.1. MS-ES+ (m/z): calculated for $C_{24}H_{40}FN_3O_4S$, 485.25 (100%), 486.28 (26.0%), 487.27 (4.5%); and found, 486.21[M+H$^+$]. The FTIR spectrum of MFTC (Figure 3.3) showed the appearance of bands at 2920 and 2860 cm^{-1} that correspond to C-H stretches of the fatty acid chain. Additionally, both palmitoyl chloride and MFTC spectra exhibited absorption bands corresponding to the carbonyl group at 1805 and 1745 cm^{-1}. XRD analysis revealed distinct diffraction patterns for FTC and MFTC suggesting different arrangement of atoms within the crystal lattice of each (Figure 3.4). Esterification of FTC decreased the aqueous solubility of the parent drug by 1200-fold (Figure 3.5A). Measurement of HIV-1 RT activity in MDMs demonstrated that MFTC did not significantly change the EC$_{50}$ of MFTC (0.033 µM) as compared to FTC (0.079 µM). These results indicated that the prodrug is efficiently hydrolyzed into the parent drug (Figure 3.5B).

3.4.2 NMFTC preparation and characterization

NMFTC was prepared by high-pressure homogenization using P407 as the stabilizing surfactant. The resultant nanoparticle size, PDI, and zeta-potential were 350 ± 10 nm, 0.24 ± 0.02, and -20 ± 2 mV, respectively, with an encapsulation efficiency of 85%. Long term stability of NMFTC was monitored at 25 °C and 4 °C. Nanoparticle size, PDI, and zeta-potential remained within acceptable range (± 10% variability) for at least 10 weeks (Figure 3.6A, B). NMFTC particle morphology was predominantly rod-shaped as shown by TEM (Figure 3.6C).

3.4.3 NMFTC-macrophage interaction

Treatment with up to 100 µM NMFTC did not affect MDM viability, as determined by the CCK-8 assay, after a 24 h exposure (Figure 3.7). This concentration was thus selected

for subsequent *in vitro* studies. Quantitation of intracellular MFTC levels showed that NMFTC was readily taken up by MDMs, reaching the highest concentration of 25 nmol/10^6 cells at 4 h followed by a rapid prodrug decay over 24 h (Figure 3.8). In contrast, exposure to FTC resulted in minimal detectable intracellular drug levels. Surprisingly, FTC was not detected in cells treated with NMFTC. These results led us to quantify intracellular levels of the active triphosphate metabolite, FTC-TP. Quantitation of FTC-TP demonstrated enhanced intracellular FTC-TP levels after exposure to NMFTC, reaching the highest concentration of 75 pmol/10^6 cells after 8 h, compared to only 10 pmol/10^6 cells for FTC exposure (Figure 3.9A). After 8 hours of NMFTC treatment then removal, intracellular FTC-TP levels were detected for up to 10 days (1.5 pmol/10^6 cells). NMFTC treatment resulted in 3-fold higher FTC-TP levels at day 5 (3.2 pmol/10^6 cells) compared to FTC treatments (Figure 3.9B). TEM showed MDM cytoplasm loaded with nanoparticles after 4 h exposure to NMFTC presumably in endosomal compartments [90, 94] (Figure 3.10).

3.4.4 Antiretroviral activities

MDMs incubated with 100 µM FTC or NMFTC for 8 hours were challenged with HIV-1$_{ADA}$ at 5-day intervals thereafter. Prior exposure to NMFTC completely inhibited viral RT activity analyzed in the cell culture medium when cells were challenged sequentially after drug preloading (Figure 3.11). This effect was reduced to 25% inhibition with NMFTC when cells were challenged 15 days after drug preloading and to 30% at 24 h with FTC. Results were confirmed in adherent cells stained for HIV-1 p24 antigen. No HIV-1 positive (brown) cells were observed in cells challenged with HIV-1$_{ADA}$ 10 days after NMFTC loading; however, HIV-1 p24+ cells were observed after a 15-day challenge. In contrast, HIV-1 p24+ cells were observed by 12 hours following native FTC treatments (Figure 3.12).

3.4.5 MFTC plasma stability

To assess the metabolic stability of MFTC in plasma, we incubated MFTC for 90 min in plasma from 6 species, namely mouse, rat, rabbit, monkey, dog, and human. MFTC rapidly declined in mouse and rat plasma, and within 30 min no detectable prodrug was observed. MFTC disappearance was slower in the plasma of other species with % decline compared to 0-min at 92% in rabbit, 33% in monkey, 20% in human and 11% in dog after 90-min of incubation (Figure 3.13A). Prodrug decay was accounted for with formation of the parent drug (FTC) as a result of ester bond hydrolysis (Figure 3.13B).

3.4.6 PK assessments

Sprague-Dawley rats were injected IM with either FTC or NMFTC at 45, 75, or 100 mg/kg FTC-equivalent doses to determine the effect of dose escalation on the PK profile. At 2h, FTC plasma levels (Figure 3.14) were several fold higher following FTC treatment compared to NMFTC treatment; however, by day 1 FTC concentrations had dropped markedly in the FTC treated animals, regardless of dose. On day 1, NMFTC provided 20-fold higher FTC plasma levels at all 3 doses compared with parent FTC (25, 34, and 52 ng/mL with FTC; 552, 696, and 1150 ng/mL with NMFTC for 45, 75 and 100 mg/kg treatments, respectively), indicating a slow release of FTC from the nanoformulation versus immediate release of the parent FTC. At day 7, NMFTC showed 11-, 14-, and 40-fold higher FTC levels with respect to the 3 doses as compared with parent FTC (0, 3, 1.4 ng/mL with FTC; 11, 42, and 55 ng/mL with NMFTC). At day 14, plasma FTC concentrations were 5-fold lower than the reported IC_{50} (i.e. 8 ng/mL) and 8-fold lower than the IC_{90} (i.e. 14 ng/mL) in all NMFTC treatment groups. Tissue FTC levels in liver, spleen, lymph nodes, and brain are shown in Figures 3.15, 3.16, 3.17, and 3.18, respectively. At day 1, NMFTC showed 11- to 28-fold higher FTC levels in all tissues compared to parent FTC. In the liver at day 7, NMFTC showed 5-, 2-, and 127-fold higher

FTC levels compared to parent FTC at the respective doses (2.6, 14, and 0.6 ng/g with FTC; 13, 27, and 76 ng/g with NMFTC). In the spleen at day 7, NMFTC showed 10-, 15-, and 10-fold higher FTC levels compared to parent FTC at the respective doses (0, 1.6, and 6 ng/g with FTC; 10, 25, and 59 ng/g with NMFTC). In lymph nodes at day 7, NMFTC showed 2-, 6-, and 13- fold higher FTC levels as compared with parent FTC at the respective doses (17, 6, and 8 ng/g with FTC; 25, 35, and 104 ng/g with NMFTC). In the brain at day 7, NMFTC showed 2-, 18-, and 10-fold higher FTC levels as compared with parent FTC at the respective doses (1.3, 1, 0.7 ng/g with FTC; 2.7, 18, 7 ng/g with NMFTC). At day 14, tissue FTC levels were detectable only in lymph nodes from the highest NMFTC dosed treatment group (36.9 ng/g).

To determine whether the active triphosphate concentrations in lymphoid cells *in vivo* would be improved by treatment of rats with NMFTC compared to FTC, FTC-TP levels in PBMCs, splenocytes and lymph node cells were determined. Intracellular FTC-TP levels in PBMCs mirrored the FTC concentrations in plasma. At 2 hours PBMC FTC-TP levels were 2-3-fold higher with parent FTC treatment compared to NMFTC treatment (Figure 3.19). However, on day 1, this was reversed and NMFTC treatment provided up to 2-fold higher FTC-TP levels compared to parent FTC (100, 133, and 163 fmol/10^6 cells with FTC; 116, 267, and 407 fmol/10^6 cells with NMFTC). At day 7, FTC-TP levels were 8-fold higher with NMFTC compared to parent FTC (6, 7, and 8 fmol/10^6 cells with FTC; 43, 60, and 64 fmol/10^6 cells with NMFTC). Intracellular FTC-TP levels in spleen and lymph nodes are shown in Figures 3.20 and 3.21, respectively. As compared to parent FTC, NMFTC treatment resulted in 2- to 4-fold higher FTC-TP levels in splenocytes and lymph node cells at days 1 and 7, respectively with all doses. FTC-TP levels in spleen at day 1 were 6-13 fmol/10^6 cells with FTC and 27-36 fmol/10^6 cells with NMFTC. These levels decreased by day 7 to 2-3 fmol/10^6 cells with FTC and 6-8 fmol/10^6 cells with NMFTC,

regardless of dose. FTC-TP levels in lymph node cells at day 1 were 4-7 fmol/10^6 cells with FTC and 8-13 fmol/10^6 cells with NMFTC. FTC-TP levels in lymph node cells dropped by day 7 to 1-2 fmol/10^6 cells with FTC and 3-4 fmol/10^6 cells with NMFTC regardless of dose. At day 14, detectable concentrations of FTC-TP in PBMCs, spleen, and lymph node cells were observed following NMFTC treatment, with the highest concentration in lymph node cells of animals treated with the highest dose (up to 2 fmol/10^6 cells). Thus, NMFTC provided slower release of the drug in plasma and significantly higher drug levels in plasma and tissues for at least 7 days compared to the parent drug. Increasing the dose resulted in higher drug levels in plasma and tissues, however, no dose-dependent differences in intracellular FTC-TP were observed.

3.5 Discussion

Since its introduction in 1996, cART has changed the clinical care landscape for HIV patients. These cART regimens have effectively decreased HIV viral load and substantially reduced disease morbidity and mortality [95]. However, due to unique viral characteristics and disease course, their management requires strict regimen adherence [96]. Moreover, rapid viral replication can often result in the emergence of mutations and drug resistance [97]. This has driven the development of new classes of drugs and alternative drug formulations that allow less frequent dosing while maintaining therapeutic drug levels in plasma and tissues.

LA ART has taken several forms. One is the development of controlled release microparticle carrier systems that rely on drug depot formation at the injection site [98]. However, these systems exhibit a tendency to aggregate due to lack of particle homogeneity leading to injection site reactions and thus limiting their usage [99]. Nanotechnology facilitates creation of formulations capable of crossing biological barriers and forming intracellular drug depots. This allows drug entry into tissues where

conventional formulations do not have access followed by subsequent slow release, as opposed to macroparticles, which tend to form injection site depots and for which local adverse reactions are very common [99].

In the current study, we developed a prodrug nanoformulation of the NRTI FTC to extend its apparent half-life and improve distribution to viral reservoir cells. FTC is an important component of initial HIV therapy as per recommendations of the International Antiviral Society-USA Panel [83]. Furthermore, FTC and TDF in combination have been shown to be effective as a PrEP prevention in high risk populations [54]. Therapeutic limitations of current FTC include a short plasma half-life, which requires once daily administration, and restriction of drug penetrance to viral reservoirs. These limitations emphasize the need for a LA parenteral nanoformulated FTC. LA therapeutics utilizing hydrophobic prodrugs have been very successful in the clinic for management of psychotic disorders [38, 100]. Our group has used similar strategies to develop hydrophobic prodrug nanoformulations of HIV integrase inhibitors CAB and dolutegravir that extended their antiretroviral efficacy for more than a month [49, 88]. Others have also reported an improvement in anti-HIV activity and cellular uptake with different FTC prodrugs; however, in contrast to our study, these FTC prodrugs were less hydrophobic, and were not delivered as nanoformulations [101]. In the current study, modification of FTC by conjugating the 16-carbon fatty acid chain, palmitoyl chloride, markedly increased the drug's hydrophobicity bringing the aqueous solubility from 134 to 0.12 mg/mL. This modification allowed for synthesis of stable nanocrystals with high encapsulation efficiency [102]. Furthermore, our method formed homogenous rod-shaped nanoparticles. Such nanoparticles have been shown to be more readily taken up my macrophages as opposed to round-shaped or spherical particles [103-105].

Macrophages are a major HIV reservoir, thus targeting macrophages for effective treatment of HIV infection has received considerable attention [106-109]. Moreover, macrophages are responsible for sustaining viral load and for spreading virus to other tissues [110, 111]. Uptake of NMFTC by MDMs was high and sustained for 10 -15 days, indicating the potential of NMFTC to target HIV reservoirs. Furthermore, macrophages could potentially be harnessed as a vehicle for drug delivery to tissues where current drugs do not have access. Interestingly, exposure of MDMs to NMFTC resulted in inhibition of viral replication after challenging the cells with HIV infection as long as 10 days after drug preloading. This result was unexpected based on our initial MDM uptake study, where no MFTC of FTC was detected by day 1 with 8-hour drug exposure. However, active FTC-TP levels showed that detectable levels were retained for up to 10 days after an 8-hour pre-exposure, which explained the *in vitro* efficacy study results. These observations were extended to *in vivo* studies, where several fold higher FTC and FTC-TP levels were present for at least 7 days in plasma, tissues, and lymphoid cells after a single NMFTC injection compared to treatment with FTC. Interestingly, the rate of hydrolysis of the prodrug and release of parent FTC was much slower in human plasma compared to rat plasma. These results suggest that this prodrug nanoformulation could be even more effective in prolonging drug residence time and efficacy in humans, due to differences in plasma esterase activities among species [112].

In summary, these studies describe the synthesis of a LA nanoformulation of a hydrophobic derivative of FTC and demonstrate that it has the potential to result in extended inhibition of HIV replication in macrophages. Higher drug levels and distribution in reticuloendothelial system and brain for longer period indicates that development of nanoparticles for anti-HIV drugs is a promising approach for improving patient adherence, long term efficacy, prevention and treatment of HIV infection. Creation of hydrophobic

prodrugs and their incorporation into nanoparticles may provide an effective way to facilitate the generation of effective and LA anti-HIV therapeutics.

3.6 Conclusions

We have demonstrated that a palmitoylated ester prodrug of FTC can extend *in vivo* drug concentrations to provide improved antiretroviral activity. The increased drug hydrophobicity facilitated formation of a P407-stabilized lipophilic nanoformulation with high drug loading efficiency. This enhanced drug uptake and antiretroviral activity in MDMs. Retention of intracellular FTC-TP provided extended antiretroviral activity of NMFTC in MDMs. Interestingly, following a single IM injection, FTC concentrations were maintained in blood, reticuloendothelial tissues, and brain for at least 7 days at significantly higher levels with NMFTC as compared with the parent drug. These results paralleled intracellular FTC-TP levels in PBMCs and in cells isolated from spleen and lymph nodes.

3.7 Figures and tables
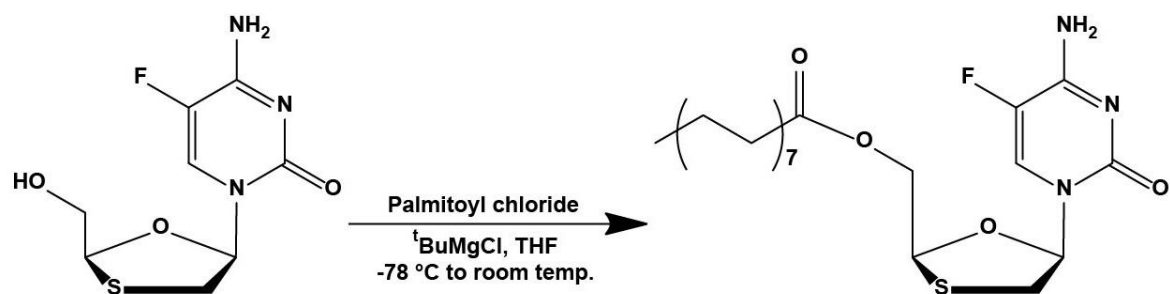
Figure 3.1 MFTC synthesis reaction. Schematic for modification of FTC with a 16-carbon palmitoyl fatty acid chain.
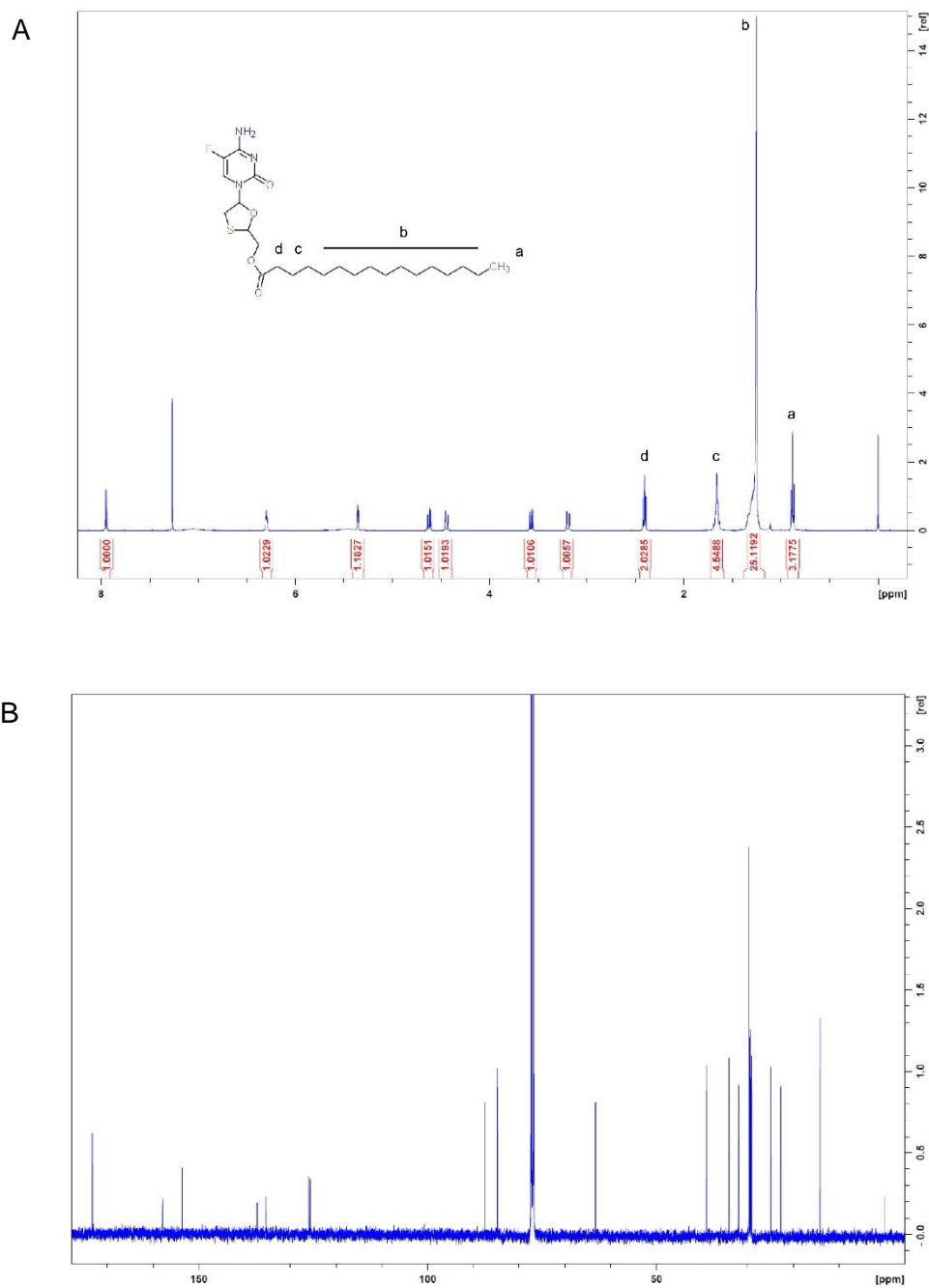
Figure 3.2 (A) ^{1}H and (B) ^{13}C- NMR spectra of MFTC in CDCl$_3$. Additional peaks corresponding to the protons and carbon atoms of the fatty acid chain confirmed derivatization of FTC.
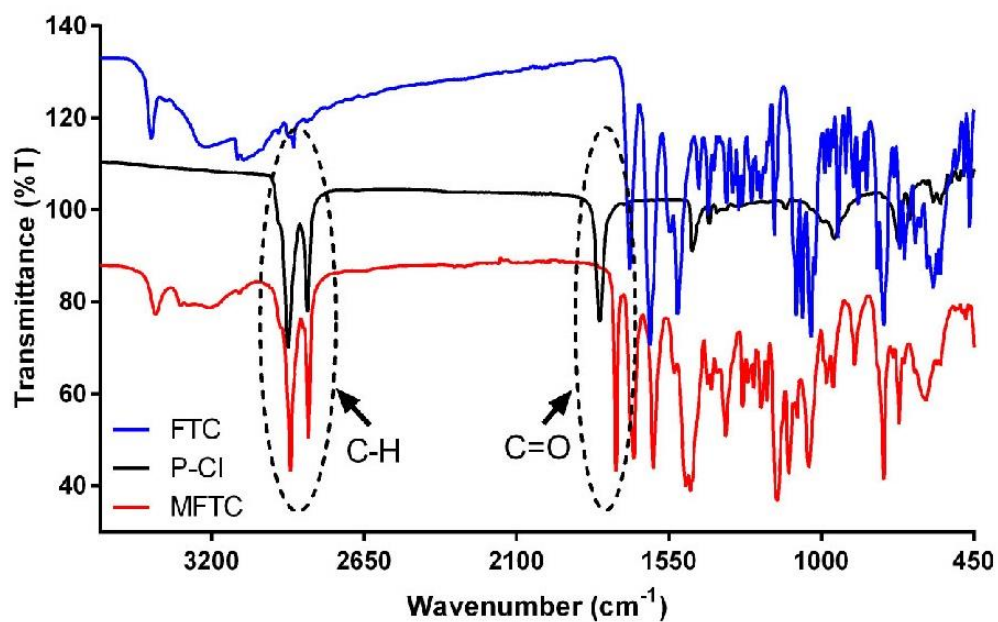
Figure 3.3 MFTC FTIR spectrum. Highlighted in dashed circles on the FTIR spectrum of MFTC are the absorption peaks at 2920 and 2860 cm^{-1} that correspond to CH_2-CH_2 stretches of the fatty acid chain and at 1745 cm^{-1} that corresponds to the carbonyl group that is part of the ester bond.
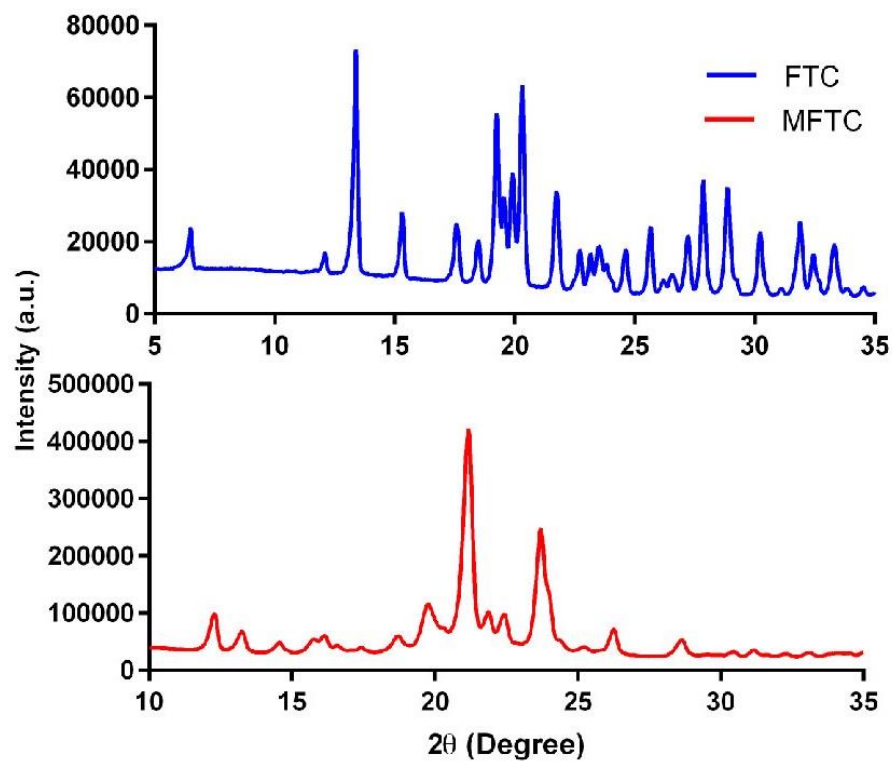
Figure 3.4 MFTC XRD spectrum. FTC and MFTC spectra show distinct diffraction patterns of both compounds indicating that they are for two different compounds; also, it indicates that the chemical modification retained the crystalline nature.
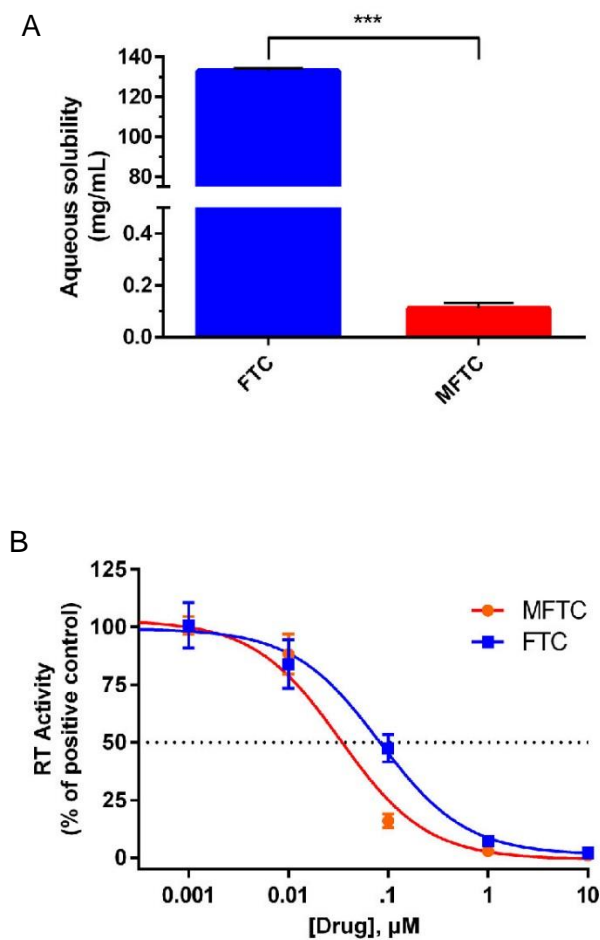
Figure 3.5 MFTC aqueous solubility and EC$_{50}$. (A) Aqueous solubility of FTC and MFTC demonstrates decrease in solubility of MFTC (mean ± SD, n = 3; ***P≤0.001). (B) EC$_{50}$ was determined *in vitro* by HIV-1 RT activity assay (0.079 and 0.033 µM for FTC and MFTC, respectively) demonstrating the chemical modification did not significantly change the antiretroviral activity of FTC. Results were analyzed by nonlinear regression fit (mean ± SD, n = 3).
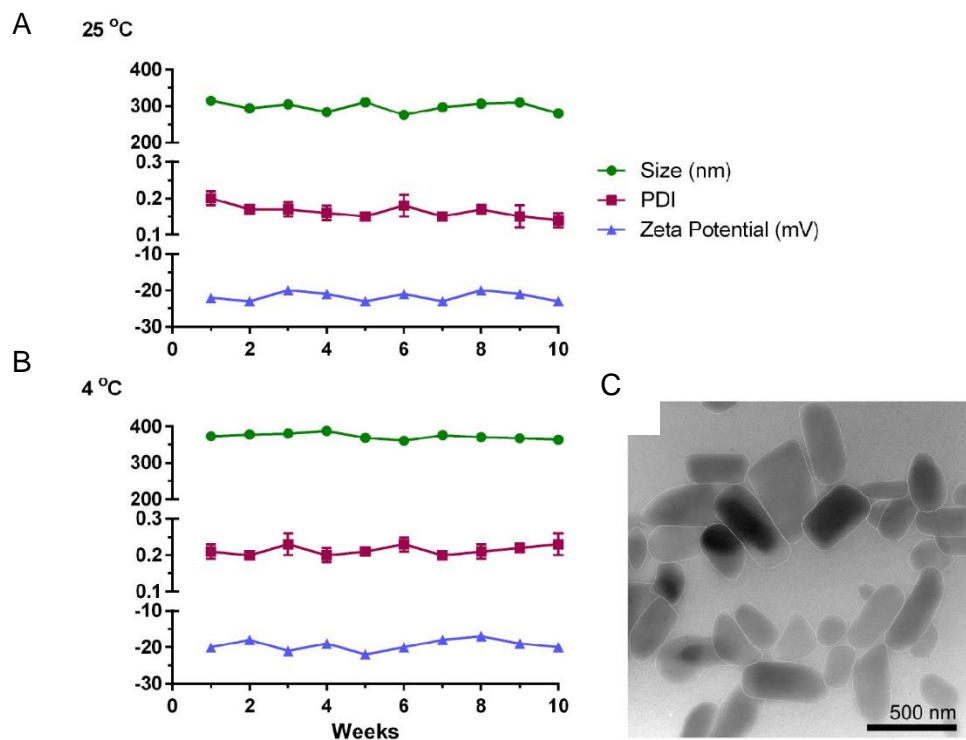
Figure 3.6 NMFTC stability and morphology. Nanoparticle stability in terms of size, PDI, and zeta-potential was measured at (A) 25 °C and (B) 4 °C. (C) TEM showed that the nanoparticles are predominantly rod-shaped. Data in A and B are shown as mean ± SD (n = 3).
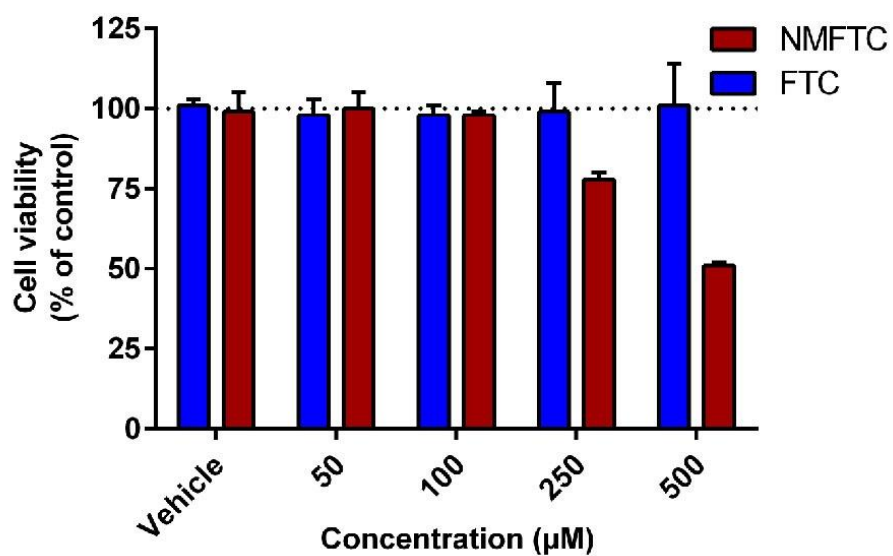
Figure 3.7 NMFTC cytotoxicity. MDMs exposed to a range of concentrations of either

FTC or NMFTC demonstrated that NMFTC has no toxicity for up to 100 μM. In contrast,

FTC is non-toxic for up to 500 μM. Data are shown as mean ± SD (n = 3).
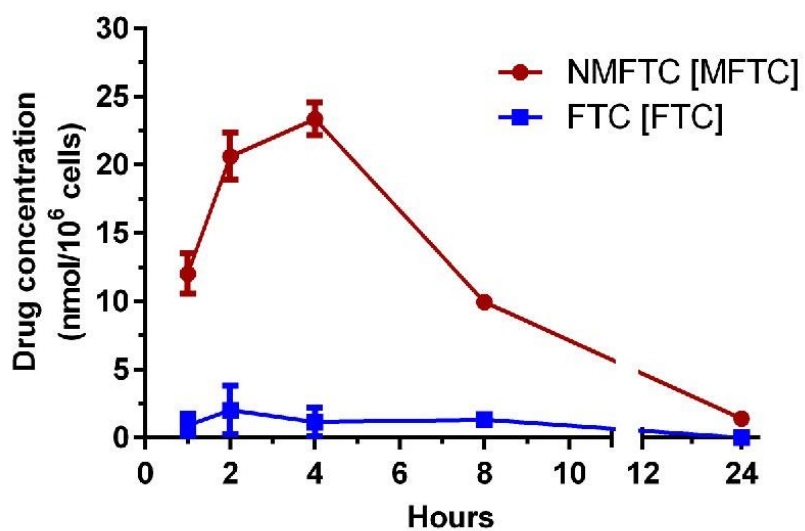
Figure 3.8 NMFTC uptake in MDMs. NMFTC was readily taken up by MDMs, with peak MFTC after 4 hours (25 nmol/10^6 cells) and declining thereafter. In contrast, FTC showed minimal uptake into MDMs. Data are means ± SD (n = 3).
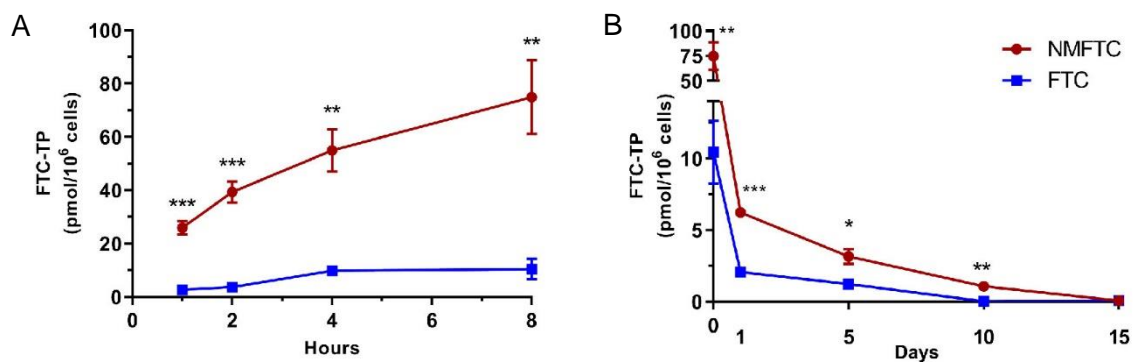
Figure 3.9 Intracellular FTC-TP levels in MDMs. (A) FTC-TP quantitation showed significantly higher concentration after exposure to NMFTC over 8 hours. (B) After 8-hour exposure, FTC-TP levels retained in MDMS for up to 10 days in significantly higher concentrations with NMFTC as compared with FTC. Data are means ± SD (n = 3).
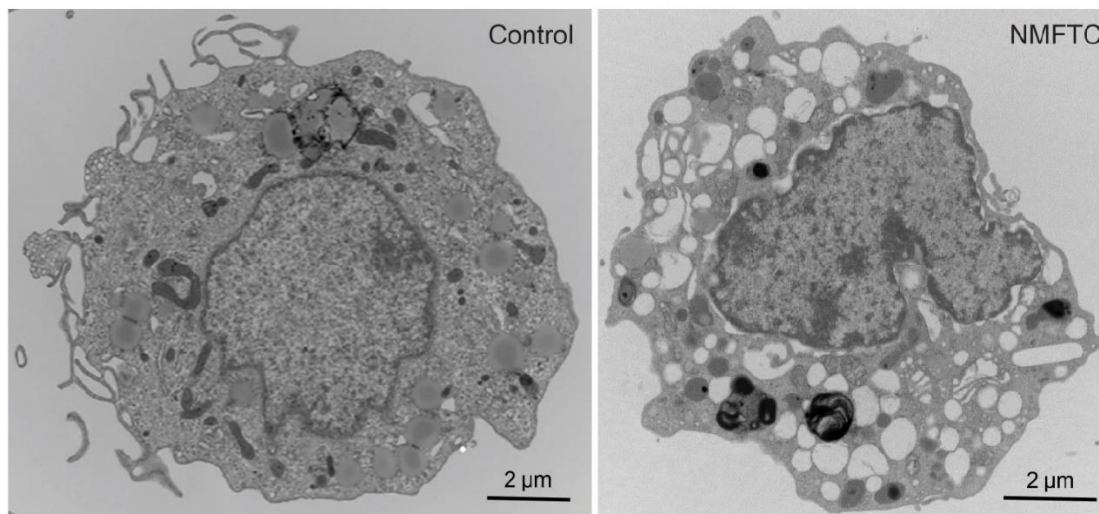
Figure 3.10 TEM of macrophage exposed to NMFTC. TEM shows macrophage cytoplasm loaded with NMFTC (white clusters) 4-hour after exposure to NMFTC.
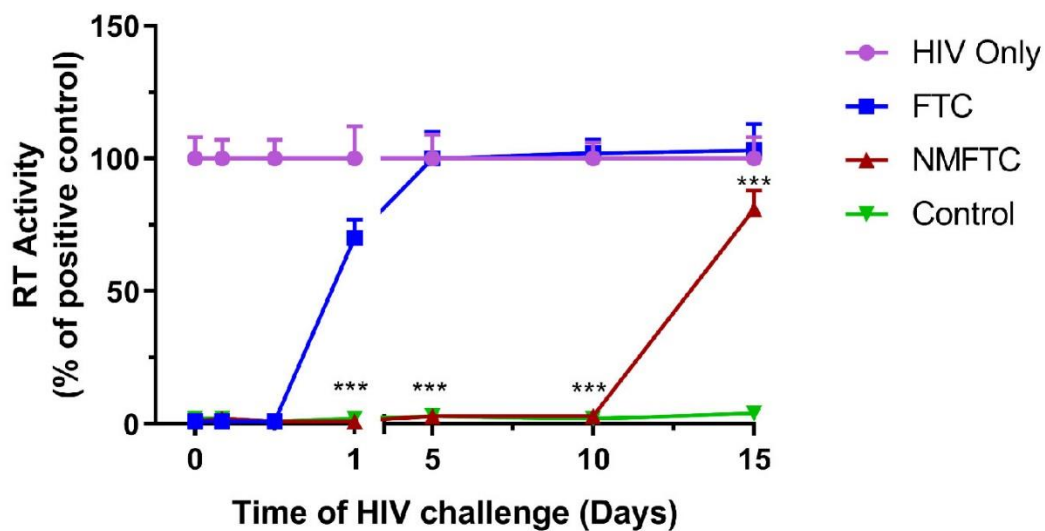
Figure 3.11 NMFTC antiretroviral activity in MDMs. NMFTC pre-exposure resulted in complete inhibition of viral RT activity after HIV-1$_{ADA}$ challenge 10 days post pre-exposure. This effect declined to 20% after challenging 15 days post pre-exposure. On the other hand, FTC pre-exposure had no effect beyond 1 day. Data are means ± SD (n = 9).
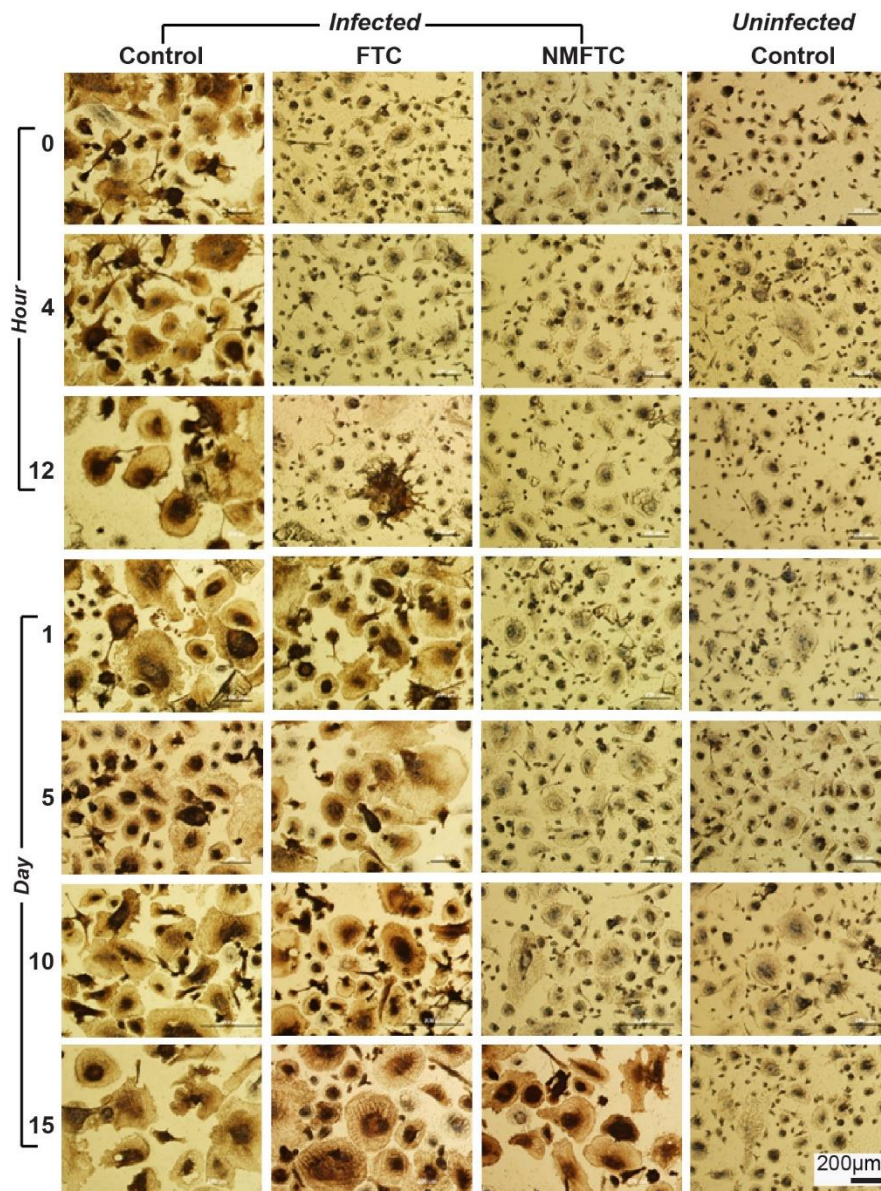
Figure 3.12 HIV-p24 antigen staining. Staining MDMs for HIV p24 antigen showed results parallel to those for RT activity in Figure 3.11. No staining was found in cells challenged 10 days after pre-exposure to NMFTC. In contrast, cells stained positive when challenged at day 1 after FTC pre-exposure.
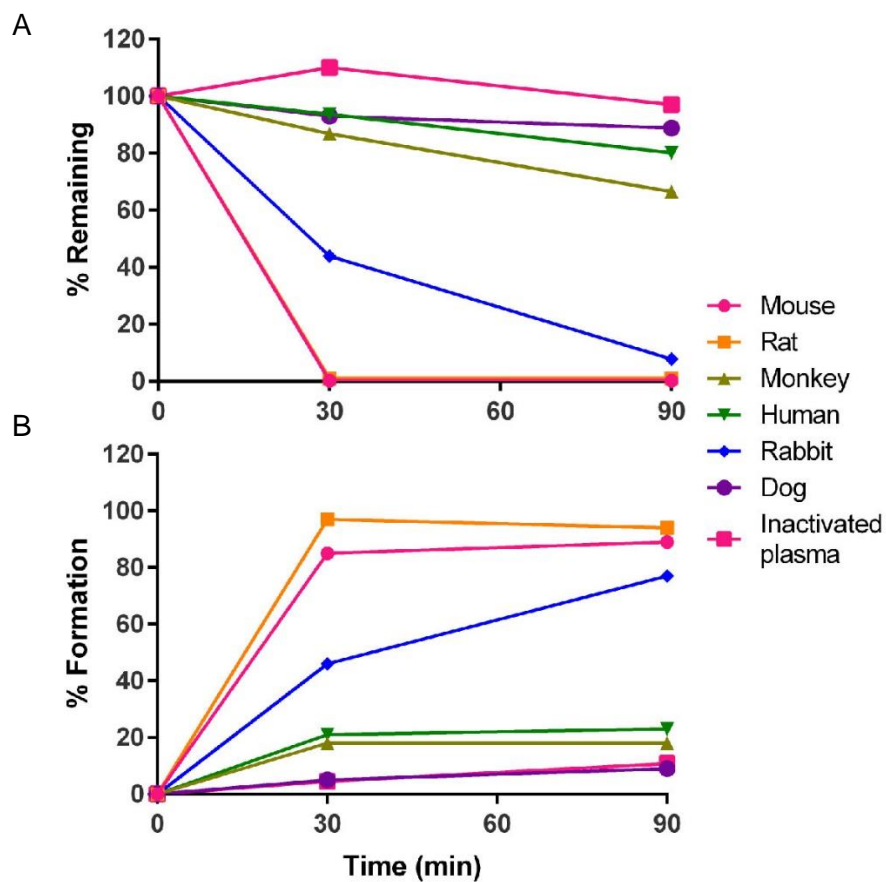
Figure 3.13 MFTC plasma stability. MFTC stability was tested in plasma of 6 different species. (A) MFTC exhibited variable hydrolysis rate being highest in mouse and rat > rabbit > monkey > human > dog. (B) Hydrolysis results were concomitant with FTC formation rate in plasma of the same species.
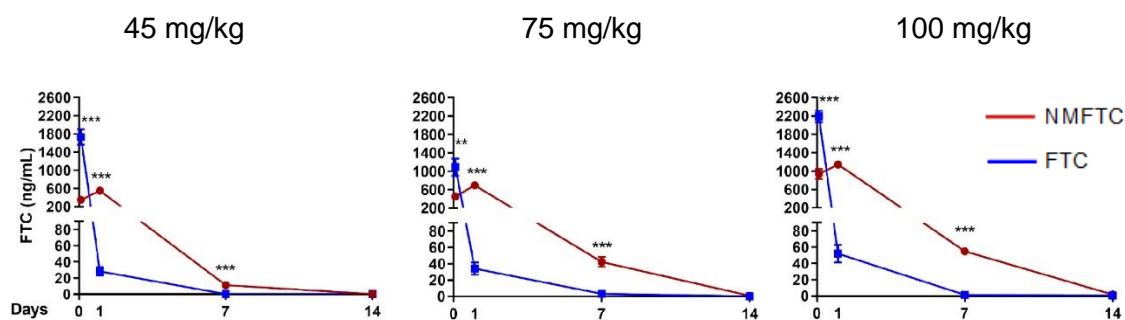
Figure 3.14 FTC concentrations in plasma. Rats were injected with 45, 75, or 100 mg/kg FTC or FTC-equivalent NMFTC. Initially at 2-hour time-point, several fold higher FTC concentrations were found in rats injected with FTC. However; this level markedly declined by day 1 where NMFTC injection showed significantly higher FTC levels for at least day 7. At day 14, drug levels were below the limit of detection. Data are means ± SEM (n = 3-5).
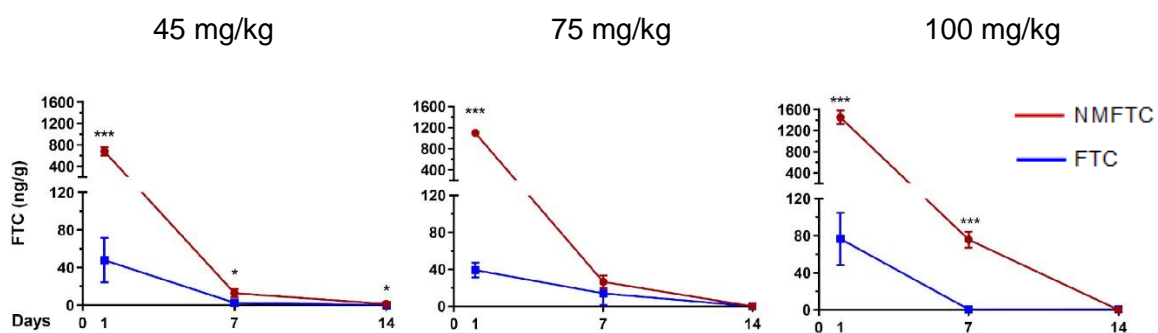
Figure 3.15 FTC concentrations in liver. Rats were injected with 45, 75, or 100 mg/kg FTC or FTC-equivalent NMFTC. Rats injected with NMFTC showed significantly higher drug levels for at least 7 days as compared to rats injected with FTC. At day 14, drug levels were below the limit of detection. Data are shown as mean ± SEM (n = 3-5).
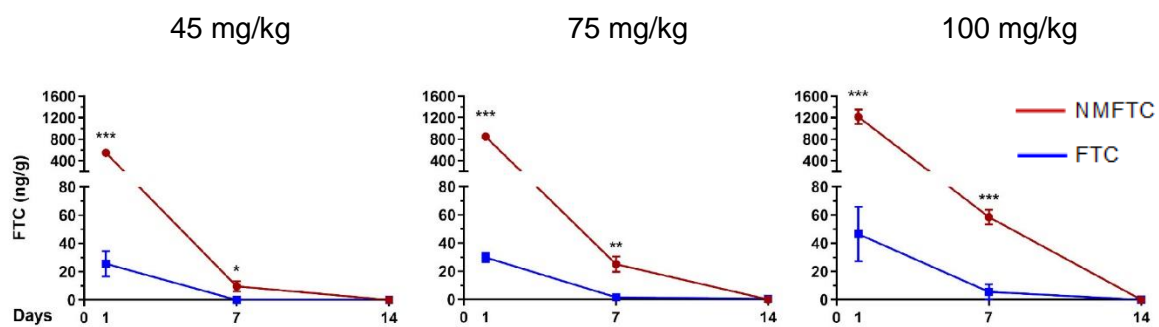
Figure 3.16 FTC concentrations in spleen. Rats were injected with 45, 75, or 100 mg/kg FTC or FTC-equivalent NMFTC. Rats injected with NMFTC showed significantly higher drug levels for at least 7 days as compared to rats injected with FTC. At day 14, drug levels were below the limit of detection. Data are means ± SEM (n = 3-5).
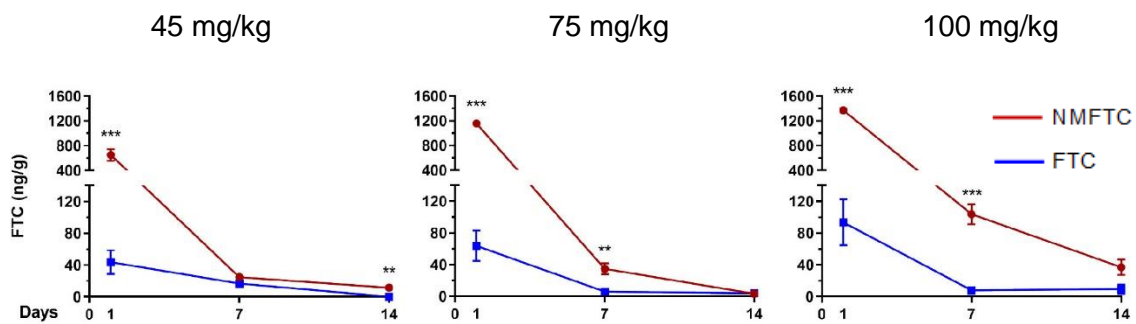
Figure 3.17 FTC concentrations in lymph nodes. Rats were injected with 45, 75, or 100 mg/kg FTC or FTC-equivalent NMFTC. Rats injected with NMFTC showed significantly higher drug levels for at least 7 days as compared to rats injected with FTC. At day 14, drug levels were below the limit of detection except with NMFTC injection at 100 mg/kg. Data are shown as mean ± SEM (n = 3-5).
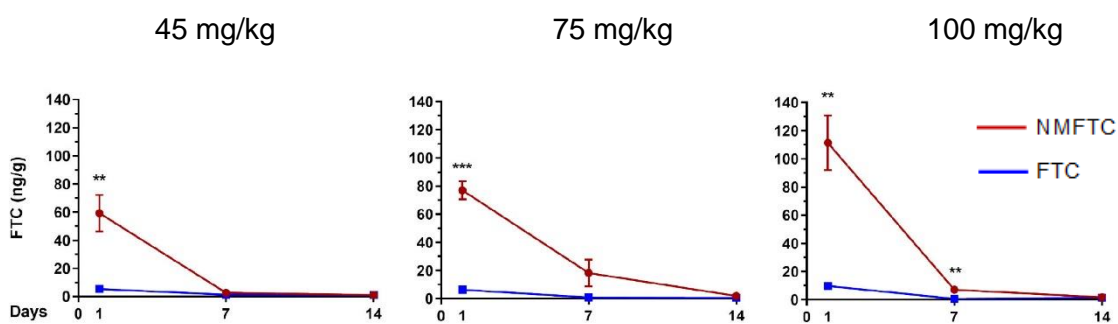
Figure 3.18 FTC concentrations in brain. Rats were injected with 45, 75, or 100 mg/kg FTC or FTC-equivalent NMFTC. Rats injected with NMFTC showed significantly higher drug levels for at least 7 days as compared to rats injected with FTC. Data are shown as mean ± SEM (n = 3-5).
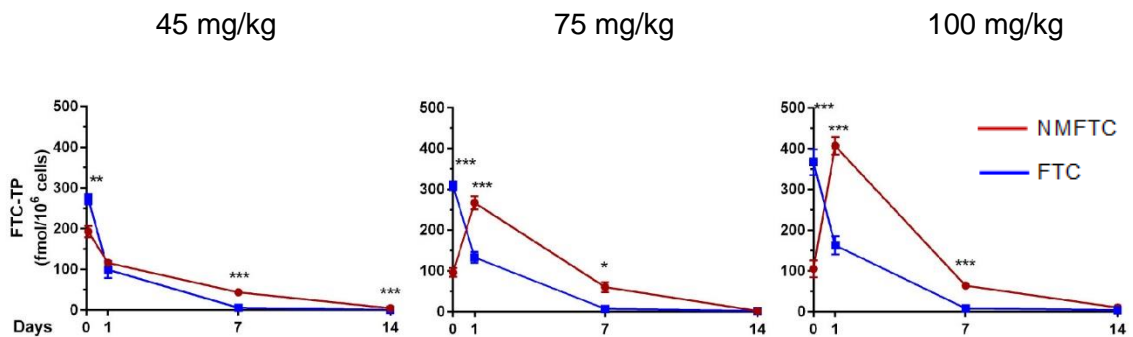
Figure 3.19 FTC-TP concentrations in PBMC. Rats were injected with 45, 75, or 100 mg/kg FTC or FTC-equivalent NMFTC. Following the same pattern observed in plasma, initially at 2-hour time-point, several fold higher FTC-TP concentrations were found in rats injected with FTC. However; this level markedly declined by day 1 where NMFTC injection showed significantly higher FTC-TP levels for at least day 7. At day 14, FTC-TP levels were below the limit of detection. Data are shown as mean ± SEM (n = 3-5).
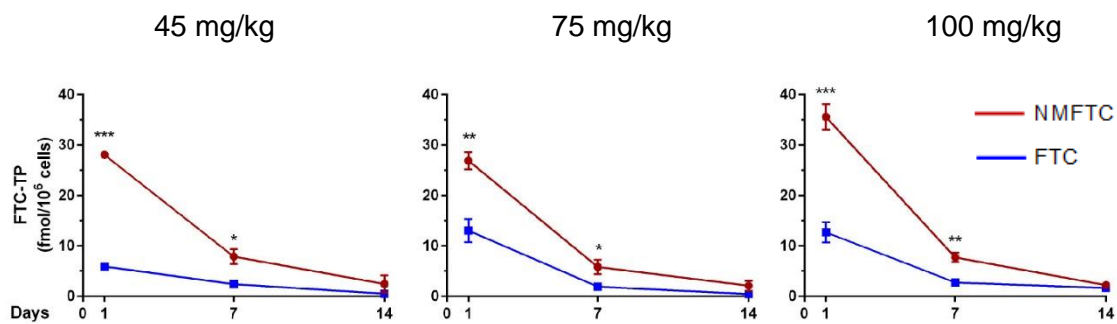
Figure 3.20 FTC-TP concentrations in splenocytes. Rats were injected with 45, 75, or 100 mg/kg FTC or FTC-equivalent NMFTC. Rats injected with NMFTC showed significantly higher FTC-TP levels for at least 7 days as compared to rats injected with FTC. At day 14, FTC-TP levels were below the limit of detection. Data are shown as mean ± SEM (n = 3-5).

45 mg/kg   75 mg/kg   100 mg/kg
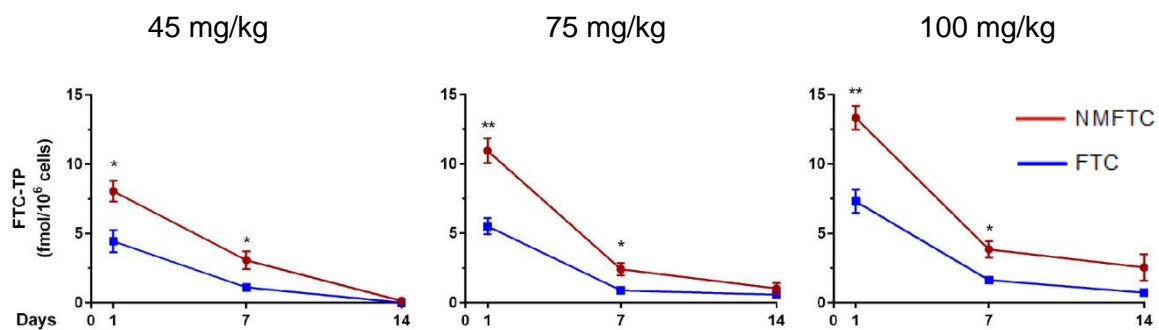
Figure 3.21 FTC-TP concentrations in lymph nodes. Rats were injected with 45, 75, or 100 mg/kg FTC or FTC-equivalent NMFTC. Rats injected with NMFTC showed significantly higher drug levels for at least 7 days as compared to rats injected with FTC. At day 14, drug levels were below the limit of detection except with NMFTC injection at 75 and 100 mg/kg. Data are shown as mean ± SEM (n = 3-5).

Chapter IV. NMFTC Pharmacodynamic Evaluation

4.1 Abstract

LA NMFTC showed promise for passively targeting MDMs, improving drug half-life, and enhancing drug biodistribution into reticuloendothelial and brain tissue as described in chapter III. To extend these studies, NMFTC, which target macrophages and permits formation of cellular drug depots, was examined using PD evaluation. To date, there are two mouse models that have been thoroughly investigated for HIV infection. Initial evaluation was done in human peripheral blood lymphocyte (hu-PBL)-reconstituted NOD/scid-IL-2Rγc^{null} (NSG) mice. Because graft-vs-host disease-induced CD4$^+$ T cell activation is common in this model, a second murine model, NSG mice reconstituted at birth with CD34+ human hematopoietic stem cells (HSC), was used to assess the efficacy of NMFTC. Unfortunately, NMFTC did not show significant protection as a PrEP measure in hu-PBL mice model. The second humanized mice model was limited because HIV challenge required longer periods to establish infection leading to inconclusive results. However, there is still potential for NMFTC to suppress HIV infection for longer periods than the parent compound. Therefore, repetition of these studies is advised, following optimization of the study protocol.

4.2 Introduction

Choosing a relevant animal model is a major hurdle, given that HIV infects only humans. HIV is specific to human immune cells and specific genetic factors critical for its replication. These include binding of HIV to immune cells via the CD4 receptor and co-receptors CCR5 and CXCR4. Attempts were made to express those receptors in murine cells, but these have not yet succeeded, which is due, in part. to absence of many factors specific to humans. Furthermore, attempts were made to generate a chimeric strain of HIV by modifying the virus itself, specifically using simian/human immunodeficiency virus (SHIV) that has been reported to replicate in monkeys [113]. Although this chimeric virus

elicits immune responses to vaccine constructs, it is different in the response that was produced with HIV infection. Limited successes were seen with some other seemingly relevant approaches, such as HIV-encoded gene expression [114]. Therefore, there is a great need to generate relevant animal models to study HIV-1 infection. In this context, humanized mice models, are reasonable alternatives.

A humanized mouse model generated by knocking down the *Prkdc* gene exhibited immunodeficiency but with leaky production of T and B cells and high production of natural killer (NK) cells. Here, knocking down recombinase activating gene 1 or (AND???) 2 (Rag1/Rag2) produced xenografts with no leaky B or T cell production. Furthermore, mutation of non-obese diabetic (NOD) mice led to a drop in the number of NK cells. Additionally, mutation of the interleukein-2 (IL-2) (gamma chain receptor) imposed a lack of IL-2 signaling in B and T cells that resulted in a more efficient xenograft. Eventually, animals with these combined mutations produced a stable engraftment referred to as NOD/scid-IL-2Rγc^{null} (NSG) mice [115]. These hu-PBL reconstituted mice are prepared by injectiion with hu-PBL intraperitonially. These mice show upregulation of human leukocyte antigen-DR (HLA-DR) and CCR5 that results in production of xeno-reactive T cells. However, due to graft-vs-host disease, these mice are prone to die. Moreover, this model is restricted by a lack of hematopoiesis, which limits their use as a chronic infection model. Despite these limitations, the ease of this model makes it suitable for acute infection studies [116].

Mice transplanted with human CD34$^+$ HSCs, on the other hand, have become promising due to graft longevity and the establishment of chronic HIV infection. These immunodeficient mice, when transplanted with HSCs, develop a functional human immune system, making them susceptible to an HIV-1 infection exhibiting natural human disease progression [117].

4.3 Materials and Methods

4.3.1 Materials

PFA, and DAB were purchased from Sigma-Aldrich (St. Louis, MO, USA). Optima grade LC/MS water and ACN were purchased from ThermoFisher Scientific (Waltham, MA, USA). FITC mouse anti-human CD45, Alexa Fluor 700 mouse anti-human CD3, APC mouse anti-human CD4, and BV421 mouse anti-human CD8 were purchased from BD Biosciences (San Jose, CA, USA). NMFTC was prepared as described in Chapter III, 3.3.3.

4.3.2 PD study in hu-PBL mouse model

Male 6-8-week-old NOD/SCID/IL2Rγc-/- (NSG) mice (Jackson Labs, Bar Harbor, ME, USA) were given intraperitoneal injection with 25×10^6 hu-PBL obtained by leukapheresis and centrifugal elutriation. Reconstitution was allowed to establish for 10 days. Then, mice were given IM injection with FTC or NMFTC at 45 mg FTC equivalents/kg. Five days following drug administration, mice were challenged with 10^4 50% tissue culture infectious doses ($TCID_{50}$) of HIV-1$_{ADA}$ by intraperitoneal injections. Mice were sacrificed 10 days after viral challenge. The experimental timeline is shown in Figure 4.1. Peripheral blood was collected in EDTA-coated tubes at days 9 (to confirm PBL reconstitution), 15 (before HIV challenge), and 25 (10 days after HIV challenge) for flow cytometry analysis of human pan-CD45, CD3, CD4 and CD8 immune cell markers [118]. Plasma was collected via centrifugation at 2,000 × g for 5 min at days 10, 21, and 32 for drug quantitation by UPLC-MS/MS. At the day of sacrifice, liver, spleen, lung, lymph nodes, bone marrow, gut, brain, and kidney were collected for drug quantitation by UPLC-MS/MS.

4.3.3 PD study in CD34+ HSC mouse model

NSG mice were reconstituted at birth with CD34+ HSCs isolated from umbilical cord blood [119]. Reconstituted mice were administered a single IM dose of FTC or NMFTC at 45 mg/kg FTC-equivalent. Mice were challenged 2 and 7 days after drug treatment with 2×10^4 $TCID_{50}$ of HIV-1$_{ADA}$ by intraperitoneal injection. Mice were sacrificed 2 weeks after HIV-1 challenge, and blood and plasma were collected to determine drug levels and viral load, respectively. The experimental timeline is shown in Figure 4.2. Plasma was used for quantifying viral load (measurements of HIV-1 RNA) using the Roche Amplicor and Taqman-48 system.

4.3.4 Viral load and HIV RNA and DNA PCR determination

HIV-1 viral load was analyzed in day 25 plasma samples using the Roche Amplicor and Taqman-48 system with HIV-1 kit V 2.0 according to the manufacturer's instructions (Roche Diagnostics, Indianapolis, USA). At the day of sacrifice, liver, spleen, lung, lymph nodes, gut, brain, and kidney were collected for viral RNA and DNA quantitation by semi-nested real-time polymerase chain reaction (PCR) [120] and for immunohistochemical staining for HIV-1p24 antigen as described previously [52].

4.4 Results

4.4.1 Viral restriction in hu-PBL mouse model

Since NMFTC demonstrated macrophage targeting and accumulation in reticuloendothelial tissues, spleen tissue was analyzed by PCR to obtain preliminary HIV-1 RNA counts. Mice challenged 5-days post drug administration showed 5 out of 6 animals harboring HIV-1 RNA comparable to infected positive controls (Figure 4.3). Mice challenged 1-day post drug administration were not analyzed, as many animals died during the study, most likely due to graft-vs-host disease, which reduced the statistical power of that group of animals.

4.4.2 Viral restriction in CD34$^+$ HSC mouse model

In this model, detection of plasma viral load in NMFTC injected animals showed complete protection in mice challenged with HIV-1 at 2 days post drug administration while FTC showed about 60% protection (Figure 4.4). In mice challenged at day 7 post treatment, 3 out of 5 animals were protected in both FTC and NMFTC treated groups. However, 3 out of 5 HIV-1 infected positive controls also did not show detectable viral load (Figure 4.5) which rendered our results inconclusive.

4.5 Discussion

No mouse model perfectly reflects human disease, so we used both hu-PBL and CD$^+$ HSC-reconstituted mouse models. Unfortunately, viral restriction as performed in hu-PBL mice failed to provide protection against viral challenge, as shown by detectable spleen viral load. This likely reflects enhancement of viral susceptibility in the animals based on the large numbers/percentages of activated lymphocytes due to xenoreactivity leading to graft-vs-host disease, timing of human cell reconstitution, larger viral challenge, route of viral challenge, and a monotherapy approach [121-124]. CD34$^+$ HSC-reconstituted NSG mice better reflect human biology, because there is no graft-vs-host disease and the reconstitution contains monocyte-macrophages, as well as CD4$^+$ and CD8$^+$ T lymphocytes [125]. To these ends, this model was used, expecting better results or to confirm results of the prior study. Indeed, cells were quiescent prior to viral challenge. Most importantly, NMFTC-treated HSC-NSG mice demonstrated plasma viral load below the limit of detection in all animals for two days after HIV-1 challenge following a single nanoparticle injection. Due to drug-related limitations, however, the time allotted to establish viral infection was not sufficient, as seen in HIV-infected control animals Based on the intrinsic properties of drug stability, *in vitro* studies in MDMs, and PK profile, such chemical prodrug modifications led to the formation of a second drug reservoir beyond the

injection site, inside macrophages. Such improvements are likely to reflect on drug PD; however, modifications to the current protocol, for example increasing the dose, are required.

4.6 Conclusions

Two different animal models were used to evaluate viral restriction after a single NMFTC IM injection. Unfortunately, majority of hu-PBL reconstituted mice that were challenged one day after drug injection died due to the limitations of this model failing this study. To overcome these limitations, we moved forward to use CD34$^+$ HSC reconstituted mouse model. However, our proposed protocol, that was based on the PK profile of NMFTC, did not give us conclusive results. We posit that further understanding and amendment of the protocol will improve future studies.

4.7 Figures
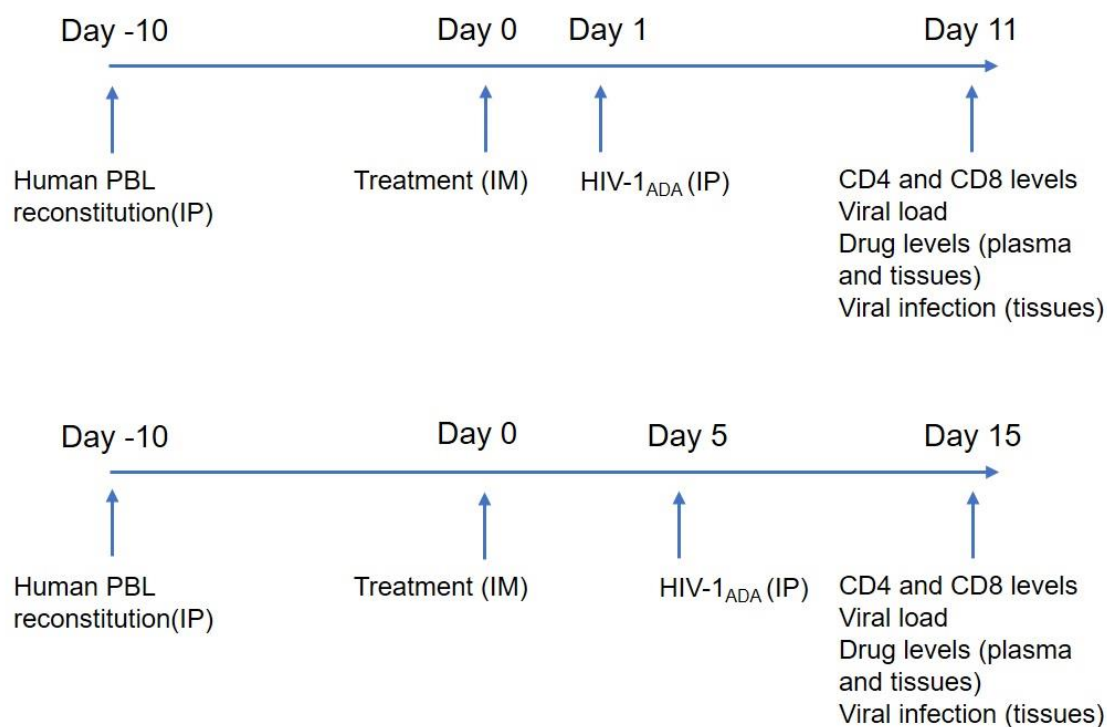
Figure 4.1. Hu-PBL reconstituted mouse model study scheme. Animals were injected with hu-PBL and reconstitution allowed to occur for 10 days. After 45 mg/kg FTC-equivalent dose administration at day 0, animals were challenged with HIV-1$_{ADA}$ at day 1 or 5. Ten days after challenge, animals were sacrificed, and blood and tissues were collected for analyses.
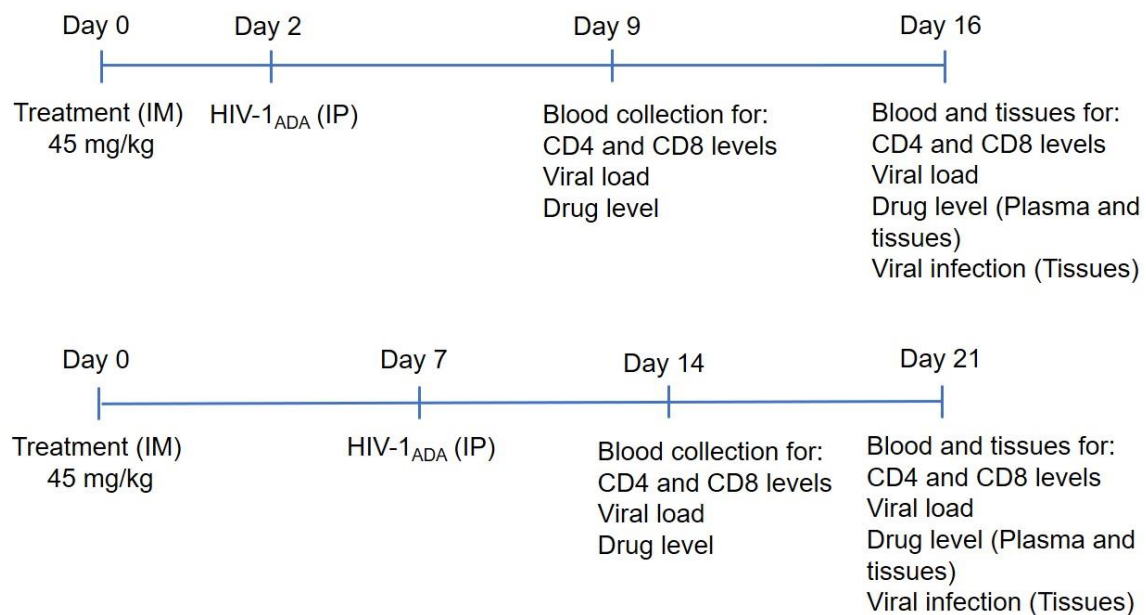
Figure 4.2. CD34+ HSC reconstituted mouse study scheme. Animals were injected with 45 mg/kg FTC-equivalent dose at day 0. Then, animals were challenged with HIV-1_{ADA} at day 2 or 7. One week after challenge, blood was collected to determine CD4 and CD8 levels, viral load, and drug levels. Two weeks after challenge, animals were sacrificed, and blood and tissues were collected for analyses.
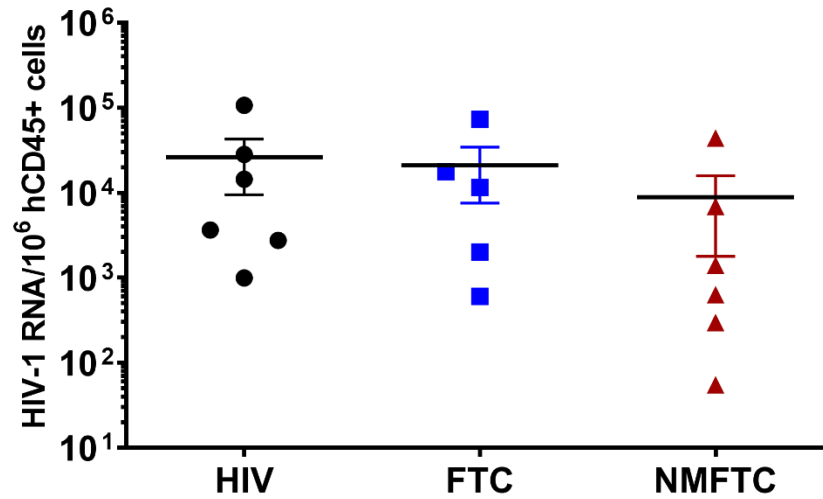
Figure 4.3 Viral load in spleen. Spleen tissues obtained from hu-PBL reconstituted mice challenged 5 days post drug administration. NMFTC did not show significant protection and results with NMFTC were comparable to FTC-treated or HIV-infected untreated controls.
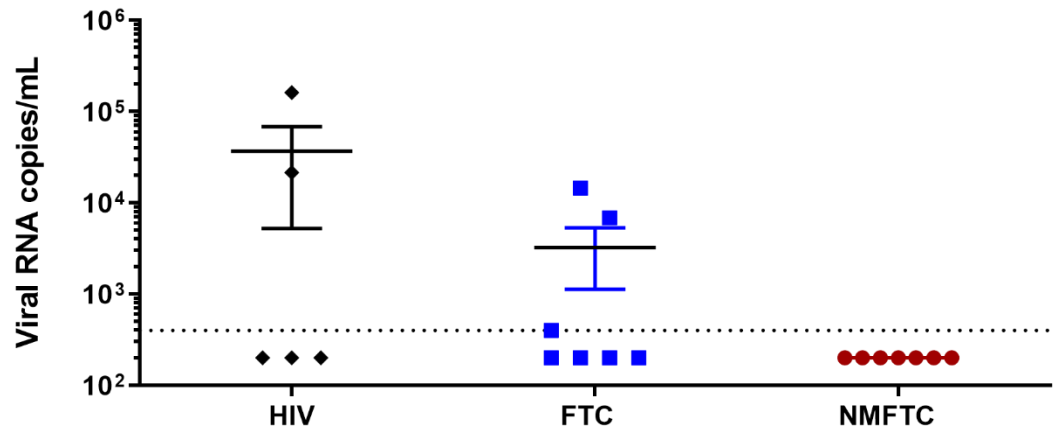
Figure 4.4 Plasma viral load after day 2 challenge. Plasma samples obtained from CD34$^+$ HSC reconstituted mice challenged 2 days post drug administration were analyzed for viral RNA. NMFTC showed complete protection as compared to only 4 out of 7 animals protected by FTC. However, 3 out of 5 positive controls did not show viral loads.
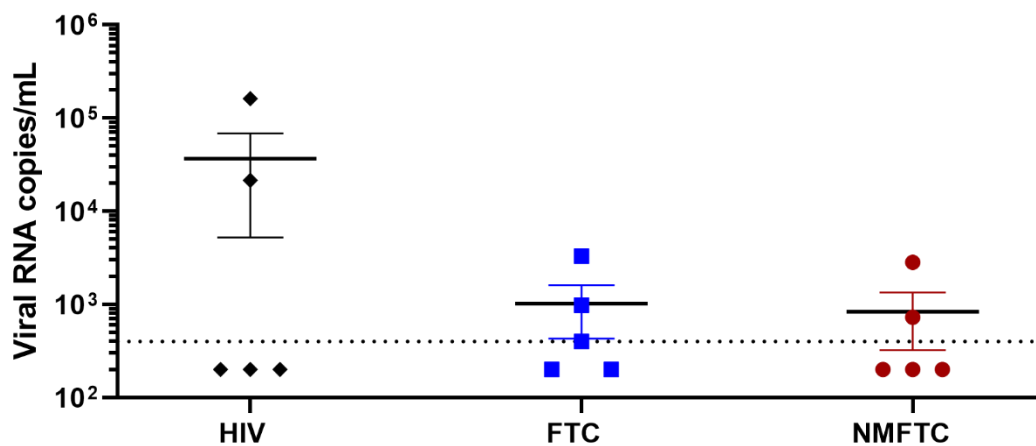
Figure 4.5 Plasma viral load after day 7 challenge. Plasma samples obtained from CD34+ HSC reconstituted mice challenged 7 days post drug administration were analyzed for HIV-1 RNA. NMFTC showed 3 out of 5 animals protected similarly to FTC. However, 3 out of 5 positive controls did not show viral loads.

Chapter V. Conclusions and Future Directions

5.1 Conclusions

Drugs formulated as nanocrystals hold promise based on their characteristic properties of size and crystalline nature to facilitate prolonged particle stability, higher dissolution rate, and improved transit across biological barriers. Selection of the excipient for making aqueous suspensions of nanocrystals is crucial to ensure particle integrity during storage and to avoid drug-related adverse reactions. Also, optimization of the manufacturing process is essential to ensure scalability. Therefore, we screened multiple poloxamers, due to their reported safety and success in pharmaceutical and biomedical industries. Although each poloxamer has unique physical properties, they did not show significant differences in terms of particle stability and MDM uptake and retention. Notably, P407 showed the highest uptake and retention in MDMs; therefore, it was chosen for further studies. High-pressure homogenization successfully prepared poloxamer-encased ATV nanosuspensions. However, purification of this nanoformulation using differential centrifugation led to particle aggregation that posed a major challenge in resuspending the particles for initial size distribution studies. Direct manufacture, on the other hand, resulted in stable and scalable particle formation.

Nanoformulation of the modified FTC prodrug, NMFTC, has the potential to overcome the limitations associated with the parent drug. In addition to prolonged shelf life, NMFTC exhibited the ability to target viral reservoirs and also longer duration as compared to parent FTC. This was demonstrated by higher drug uptake by macrophages, longer circulation time, and higher drug biodistribution in reticuloendothelial tissues along with higher intracellular FTC-TP concentrations. However, translation of these results into viral restriction in animal models requires thorough understanding of the available HIV-1 infection models and optimization of the study protocol accordingly.

5.2 Challenges and future directions

The current project has provided improvements in the PK profile of FTC and multiple steps forward toward making LA ART formulations of NRTIs. Further improvements are needed to extend the PK profile beyond 7 days. This challenge can be tackled by combining ligand-based active targeting to HIV reservoirs. Preliminary studies in our laboratory have demonstrated that incorporation of FA on the nanoparticle could further improve macrophage uptake [50]. Other targeting ligands that target macrophages or CD4$^+$ cells, such as hyaluronic acid [126], tuftsin [127], gp120 peptide [128], and others, are currently being tested.

LA formulations and devices are being developed to provide sustained release ART for prevention and treatment of HIV-1 infection. Ideal drug candidates for LA delivery require extremely potent and hydrophobic molecules. However, most ARVs used in combination therapy are either too hydrophilic or require high dosage, limiting their potential transition into LA agents. Recent advances in prodrug and nanotechnology approaches present an attractive option to overcome the undesirable properties of existing ARVs. While ester prodrugs of NRTIs such as MFTC represent a first step towards extending the half-life of hydrophilic compounds, another strategy, known as ProTide, can be investigated to further enhance drug potency and to sustain active triphosphate levels at restricted sites of infection. The ProTide strategy is based on delivery of a monophosphate derivative of an NRTI, bypassing the rate-limiting first phosphorylation step. Furthermore, this can be coupled with conjugation of fatty acid esters to make LA formulations, as we have shown in the current study.

Bibliography

1.   *World Health Organization.* 3/21/2019]; Available from: https://www.who.int/gho/hiv/en/.
2.   *Global HIV & AIDS statistics - 2018 fact sheets.* 3/5/2019]; Available from: http://www.unaids.org/en/resources/fact-sheet.
3.   Control, C.f.D., *Kaposi's sarcoma and Pneumocystis pneumonia among homosexual men--New York City and California.* MMWR. Morbidity and mortality weekly report, 1981. **30**(25): p. 305.
4.   Control, C.f.D., *Pneumocystis pneumonia Los Angeles.* MMwR, 1981. **30**: p. 250-252.
5.   Levy, J.A., *Pathogenesis of human immunodeficiency virus infection.* Microbiology and Molecular Biology Reviews, 1993. **57**(1): p. 183-289.
6.   Fauci, A.S., *HIV and AIDS: 20 years of science.* Nature medicine, 2003. **9**(7): p. 839.
7.   Li, G. and E. De Clercq, *HIV Genome-Wide Protein Associations: a Review of 30 Years of Research.* Microbiology and Molecular Biology Reviews, 2016. **80**(3): p. 679-731.
8.   Endres, M.J., et al., *CD4-independent infection by HIV-2 is mediated by fusin/CXCR4.* Cell, 1996. **87**(4): p. 745-756.
9.   Doranz, B.J., et al., *A dual-tropic primary HIV-1 isolate that uses fusin and the beta-chemokine receptors CKR-5, CKR-3, and CKR-2b as fusion cofactors.* Cell, 1996. **85**(7): p. 1149-58.
10.   Choe, H., et al., *The beta-chemokine receptors CCR3 and CCR5 facilitate infection by primary HIV-1 isolates.* Cell, 1996. **85**(7): p. 1135-48.
11.   Merk, A. and S. Subramaniam, *HIV-1 envelope glycoprotein structure.* Current opinion in structural biology, 2013. **23**(2): p. 268-276.
12.   Campbell, E.M. and T.J. Hope, *HIV-1 capsid: the multifaceted key player in HIV-1 infection.* Nature reviews. Microbiology, 2015. **13**(8): p. 471-483.
13.   Chitwood, D.D., et al., *HIV seropositivity of needles from shooting galleries in south Florida.* American journal of public health, 1990. **80**(2): p. 150-152.
14.   Fry, D.E., *Occupational risks of blood exposure in the operating room.* The American surgeon, 2007. **73**(7): p. 637-646.
15.   Kuhar, D.T., et al., *Updated US Public Health Service guidelines for the management of occupational exposures to human immunodeficiency virus and recommendations for postexposure prophylaxis.* Infection Control & Hospital Epidemiology, 2013. **34**(9): p. 875-892.
16.   Ancelle, R., et al., *Long incubation period for HIV-2 infection.* Lancet, 1987. **1**(8534): p. 688-9.
17.   Fang, R.H.T., A.D. Colantonio, and C.H. Uittenbogaart, *The role of the thymus in HIV infection: a 10 year perspective.* Aids, 2008. **22**(2): p. 171-184.
18.   Nilsson, J., et al., *Early immune activation in gut-associated and peripheral lymphoid tissue during acute HIV infection.* Aids, 2007. **21**(5): p. 565-574.
19.   Castro, K.G., et al., *1993 revised classification system for HIV infection and expanded surveillance case definition for AIDS among adolescents and adults.* Clinical Infectious Diseases, 1993. **17**(4): p. 802-810.
20.   Saag, M.S., et al., *Antiretroviral drugs for treatment and prevention of HIV infection in adults: 2018 recommendations of the International Antiviral Society–USA Panel.* Jama, 2018. **320**(4): p. 379-396.

21.   Poveda, E., V. Briz, and V. Soriano, *HIV entry inhibitors: mechanisms of action and resistance pathways.* Journal of Antimicrobial Chemotherapy, 2006. **57**(4): p. 619-627.

22.   Hurwitz, S.J. and R.F. Schinazi, *Practical Considerations For Developing Nucleoside Reverse Transcriptase Inhibitors.* Drug discovery today. Technologies, 2012. **9**(3): p. e183-e193.

23.   Kohler, J.J. and W. Lewis, *A brief overview of mechanisms of mitochondrial toxicity from NRTIs.* Environmental and Molecular Mutagenesis, 2007. **48**(3-4): p. 166-172.

24.   Usach, I., V. Melis, and J.E. Peris, *Non-nucleoside reverse transcriptase inhibitors: a review on pharmacokinetics, pharmacodynamics, safety and tolerability.* J Int AIDS Soc, 2013. **16**(1): p. 1-14.

25.   Flexner, C., *HIV-Protease Inhibitors.* New England Journal of Medicine, 1998. **338**(18): p. 1281-1293.

26.   Petruschke, R.A. and R.K. Zeldin, *Pharmacological and therapeutic properties of ritonavir-boosted protease inhibitor therapy in HIV-infected patients.* Journal of Antimicrobial Chemotherapy, 2004. **53**(1): p. 4-9.

27.   Fogarty, L., et al., *Patient adherence to HIV medication regimens: a review of published and abstract reports.* Patient Education and Counseling, 2002. **46**(2): p. 93-108.

28.   Dahabieh, M.S., E. Battivelli, and E. Verdin, *Understanding HIV Latency: The Road to an HIV Cure.* Annual Review of Medicine, 2015. **66**(1): p. 407-421.

29.   Alòs, L., et al., *Immunoarchitecture of lymphoid tissue in HIV-infection during antiretroviral therapy correlates with viral persistence.* Modern Pathology, 2004. **18**: p. 127.

30.   Alexaki, A., Y. Liu, and B. Wigdahl, *Cellular reservoirs of HIV-1 and their role in viral persistence.* Current HIV research, 2008. **6**(5): p. 388-400.

31.   Lorenzo-Redondo, R., et al., *Persistent HIV-1 replication maintains the tissue reservoir during therapy.* Nature, 2016. **530**(7588): p. 51.

32.   Smith, M.Z., F. Wightman, and S.R. Lewin, *HIV reservoirs and strategies for eradication.* Current HIV/AIDS Reports, 2012. **9**(1): p. 5-15.

33.   Curtis, K.M. and J.F. Peipert, *Long-acting reversible contraception.* New England Journal of Medicine, 2017. **376**(5): p. 461-468.

34.   Cirincione, B., J. Edwards, and D.E. Mager, *Population Pharmacokinetics of an Extended-Release Formulation of Exenatide Following Single- and Multiple-Dose Administration.* Aaps j, 2017. **19**(2): p. 487-496.

35.   Cioppi, F., et al., *The LARO-MEN1 study: a longitudinal clinical experience with octreotide Long-Acting Release in patients with Multiple Endocrine Neoplasia type 1 Syndrome.* Clin Cases Miner Bone Metab, 2017. **14**(2): p. 123-130.

36.   Bakshi, R.P., et al., *Long-acting injectable atovaquone nanomedicines for malaria prophylaxis.* Nat Commun, 2018. **9**(1): p. 315.

37.   Swindells, S., et al., *Long-acting formulations for the treatment of latent tuberculous infection: opportunities and challenges.* Int J Tuberc Lung Dis, 2018. **22**(2): p. 125-132.

38.   Ravenstijn, P., et al., *Pharmacokinetics, safety, and tolerability of paliperidone palmitate 3-month formulation in patients with schizophrenia: A phase-1, single-dose, randomized, open-label study.* the journal of clinical pharmacology, 2016. **56**(3): p. 330-339.

39.   Williams, J., et al., *Long-acting parenteral nanoformulated antiretroviral therapy: interest and attitudes of HIV-infected patients.* Nanomedicine, 2013. **8**(11): p. 1807-1813.

40. van der Straten, A., et al., *Perspectives on use of oral and vaginal antiretrovirals for HIV prevention: the VOICE-C qualitative study in Johannesburg, South Africa.* Journal of the International AIDS Society, 2014. **17**: p. 19146.

41. Hickey, M.B., et al., *Delivery of long-acting injectable antivirals: best approaches and recent advances.* Curr Opin Infect Dis, 2015. **28**(6): p. 603-10.

42. Park, E.J., et al., *Long-acting injectable formulations of antipsychotic drugs for the treatment of schizophrenia.* Archives of pharmacal research, 2013. **36**(6): p. 651-659.

43. Koseki, Y., et al., *Drug release is determined by the chain length of fatty acid-conjugated anticancer agent as one component of nano-prodrug.* Bulletin of the Chemical Society of Japan, 2016. **89**(5): p. 540-545.

44. Zhou, H., et al., *Hydrophobic ion pairing of isoniazid using a prodrug approach.* Journal of pharmaceutical sciences, 2002. **91**(6): p. 1502-1511.

45. Rabinow, B.E., *Nanosuspensions in drug delivery.* Nature reviews Drug discovery, 2004. **3**(9): p. 785.

46. Lamb, Y.N. and G.M. Keating, *Paliperidone palmitate intramuscular 3-monthly formulation: a review in schizophrenia.* Drugs, 2016. **76**(16): p. 1559-1566.

47. Batrakova, E.V., H.E. Gendelman, and A.V. Kabanov, *Cell-mediated drug delivery.* Expert opinion on drug delivery, 2011. **8**(4): p. 415-433.

48. Singh, D., et al., *Development and characterization of a long-acting nanoformulated abacavir prodrug.* Nanomedicine, 2016. **11**(15): p. 1913-1927.

49. Sillman, B., et al., *Creation of a long-acting nanoformulated dolutegravir.* Nature communications, 2018. **9**(1): p. 443.

50. Zhou, T., et al., *Creation of a nanoformulated cabotegravir prodrug with improved antiretroviral profiles.* Biomaterials, 2018. **151**: p. 53-65.

51. Guo, D., et al., *Creation of a long-acting nanoformulated 2', 3'-dideoxy-3'-thiacytidine.* Journal of acquired immune deficiency syndromes (1999), 2017. **74**(3): p. e75.

52. Puligujja, P., et al., *Pharmacodynamics of long-acting folic acid-receptor targeted ritonavir-boosted atazanavir nanoformulations.* Biomaterials, 2015. **41**: p. 141-150.

53. Nelson, M. and M. Schiavone, *Emtricitabine (FTC) for the treatment of HIV infection.* International journal of clinical practice, 2004. **58**(5): p. 504-510.

54. McCormack, S., et al., *Pre-exposure prophylaxis to prevent the acquisition of HIV-1 infection (PROUD): effectiveness results from the pilot phase of a pragmatic open-label randomised trial.* The Lancet, 2016. **387**(10013): p. 53-60.

55. Van der Elst, E.M., et al., *High acceptability of HIV pre-exposure prophylaxis but challenges in adherence and use: qualitative insights from a phase I trial of intermittent and daily PrEP in at-risk populations in Kenya.* AIDS and Behavior, 2013. **17**(6): p. 2162-2172.

56. Volberding, P.A. and S.G. Deeks, *Antiretroviral therapy and management of HIV infection.* The Lancet, 2010. **376**(9734): p. 49-62.

57. Fauci, A.S., *Host factors and the pathogenesis of HIV-induced disease.* Nature, 1996. **384**(6609): p. 529-34.

58. Dolgin, E., *Long-acting HIV drugs advanced to overcome adherence challenge.* 2014, Nature Publishing Group.

59. Margolis, D.A., et al., *Long-acting intramuscular cabotegravir and rilpivirine in adults with HIV-1 infection (LATTE-2): 96-week results of a randomised, open-label, phase 2b, non-inferiority trial.* The Lancet, 2017. **390**(10101): p. 1499-1510.

60.   Trezza, C., et al., *Formulation and pharmacology of long-acting cabotegravir.* Current opinion in HIV and AIDS, 2015. **10**(4): p. 239.

61.   Williams, P.E., H.M. Crauwels, and E.D. Basstanie, *Formulation and pharmacology of long-acting rilpivirine.* Current Opinion in HIV and AIDS, 2015. **10**(4): p. 233-238.

62.   Markowitz, M., et al., *Safety and tolerability of long-acting cabotegravir injections in HIV-uninfected men (ECLAIR): a multicentre, double-blind, randomised, placebo-controlled, phase 2a trial.* The Lancet HIV, 2017. **4**(8): p. e331-e340.

63.   McGowan, I., et al., *Long-acting rilpivirine as potential pre-exposure prophylaxis for HIV-1 prevention (the MWRI-01 study): an open-label, phase 1, compartmental, pharmacokinetic and pharmacodynamic assessment.* The Lancet HIV, 2016. **3**(12): p. e569-e578.

64.   Lin, S.-Y. and Y. Kawashima, *The influence of three poly (oxyethylene) poly (oxypropylene) surface-active block copolymers on the solubility behavior of indomethacin.* Pharmaceutica Acta Helvetiae, 1985. **60**(12): p. 339.

65.   Kabanov, A.V., E.V. Batrakova, and D.W. Miller, *Pluronic® block copolymers as modulators of drug efflux transporter activity in the blood–brain barrier.* Advanced Drug Delivery Reviews, 2003. **55**(1): p. 151-164.

66.   Liversidge, G.G. and K.C. Cundy, *Particle size reduction for improvement of oral bioavailability of hydrophobic drugs: I. Absolute oral bioavailability of nanocrystalline danazol in beagle dogs.* International journal of pharmaceutics, 1995. **125**(1): p. 91-97.

67.   Hu, J., K.P. Johnston, and R.O. Williams III, *Nanoparticle engineering processes for enhancing the dissolution rates of poorly water soluble drugs.* Drug development and industrial pharmacy, 2004. **30**(3): p. 233-245.

68.   Chen, Y., et al., *Oleanolic acid nanosuspensions: preparation, in-vitro characterization and enhanced hepatoprotective effect.* Journal of Pharmacy and Pharmacology, 2005. **57**(2): p. 259-264.

69.   Arunkumar, N., M. Deecaraman, and C. Rani, *Nanosuspension technology and its applications in drug delivery.* Asian journal of pharmaceutics, 2009. **3**(3): p. 168.

70.   Gendelman, H.E., et al., *Efficient isolation and propagation of human immunodeficiency virus on recombinant colony-stimulating factor 1-treated monocytes.* Journal of Experimental Medicine, 1988. **167**(4): p. 1428-1441.

71.   Zhou, T., *Next Generation of Translational Long-Acting Cabotegravir.* 2018.

72.   Nyaku, A.N., S.G. Kelly, and B.O. Taiwo, *Long-acting antiretrovirals: where are we now?* Current HIV/AIDS Reports, 2017. **14**(2): p. 63-71.

73.   Loureiro, A., et al., *Albumin-based nanodevices as drug carriers.* Current pharmaceutical design, 2016. **22**(10): p. 1371-1390.

74.   Edagwa, B., et al., *Long-acting slow effective release antiretroviral therapy.* Expert opinion on drug delivery, 2017. **14**(11): p. 1281-1291.

75.   Pirrone, V., et al., *Combinatorial approaches to the prevention and treatment of HIV-1 infection.* Antimicrobial Agents and Chemotherapy, 2011. **55**(5): p. 1831-1842.

76.   Bangsberg, D.R., et al., *Non-adherence to highly active antiretroviral therapy predicts progression to AIDS.* Aids, 2001. **15**(9): p. 1181-1183.

77.   Rueda, S., et al., *Patient support and education for promoting adherence to highly active antiretroviral therapy for HIV/AIDS.* Cochrane database of systematic reviews, 2006(3).

78.   Chesney, M., *Adherence to HAART regimens.* AIDS Patient Care and STDs, 2003. **17**(4): p. 169-177.

79. Chun, T.W., S. Moir, and A.S. Fauci, *HIV reservoirs as obstacles and opportunities for an HIV cure.* Nature immunology, 2015. **16**(6): p. 584-589.

80. Barnhart, M., *Long-Acting HIV Treatment and Prevention: Closer to the Threshold.* Global health, science and practice, 2017. **5**(2): p. 182-187.

81. Meltzer, M.S., et al., *Macrophages and the human immunodeficiency virus.* Immunology today, 1990. **11**: p. 217-223.

82. Dou, H., et al., *Development of a macrophage-based nanoparticle platform for antiretroviral drug delivery.* Blood, 2006. **108**(8): p. 2827-2835.

83. Saag, M.S., et al., *Antiretroviral Drugs for Treatment and Prevention of HIV Infection in Adults: 2018 Recommendations of the International Antiviral Society-USA Panel.* Jama, 2018. **320**(4): p. 379-396.

84. Bruno, R., et al., *Comparison of the plasma pharmacokinetics of lamivudine during twice and once daily administration in patients with HIV.* Clinical pharmacokinetics, 2001. **40**(9): p. 695-700.

85. Ruane, P.J., et al., *Antiviral Activity, Safety, and Pharmacokinetics/Pharmacodynamics of Tenofovir Alafenamide as 10-Day Monotherapy in HIV-1–Positive Adults.* JAIDS Journal of Acquired Immune Deficiency Syndromes, 2013. **63**(4): p. 449-455.

86. Richman, D.D., *Antiretroviral activity of emtricitabine, a potent nucleoside reverse transcriptase inhibitor.* Antiviral therapy, 2001. **6**(2): p. 83-88.

87. Singh, D., et al., *Development and characterization of a long-acting nanoformulated abacavir prodrug.* Nanomedicine (London, England), 2016. **11**(15): p. 1913-1927.

88. Zhou, T., et al., *Creation of a nanoformulated cabotegravir prodrug with improved antiretroviral profiles.* Biomaterials, 2018. **151**: p. 53-65.

89. Piliero, P.J., *Pharmacokinetic properties of nucleoside/nucleotide reverse transcriptase inhibitors.* Journal of acquired immune deficiency syndromes (1999), 2004. **37 Suppl 1**: p. S2-S12.

90. Arainga, M., et al., *Opposing regulation of endolysosomal pathways by long-acting nanoformulated antiretroviral therapy and HIV-1 in human macrophages.* Retrovirology, 2015. **12**: p. 5-014-0133-5.

91. Gendelman, H.E., et al., *Efficient isolation and propagation of human immunodeficiency virus on recombinant colony-stimulating factor 1-treated monocytes.* The Journal of experimental medicine, 1988. **167**(4): p. 1428-1441.

92. Gautam, N., et al., *Simultaneous quantification of intracellular lamivudine and abacavir triphosphate metabolites by LC–MS/MS.* Journal of pharmaceutical and biomedical analysis, 2018. **153**: p. 248-259.

93. Li, F., H. Maag, and T. Alfredson, *Prodrugs of nucleoside analogues for improved oral absorption and tissue targeting.* Journal of pharmaceutical sciences, 2008. **97**(3): p. 1109-1134.

94. Guo, D., et al., *Endosomal trafficking of nanoformulated antiretroviral therapy facilitates drug particle carriage and HIV clearance.* J Virol, 2014. **88**(17): p. 9504-13.

95. Carpenter, C.C., et al., *Antiretroviral therapy for HIV infection in 1997: updated recommendations of the International AIDS Society—USA Panel.* Jama, 1997. **277**(24): p. 1962-1969.

96. Friedland, G.H. and A. Williams, *Attaining higher goals in HIV treatment: The central importance of adherence.* AIDS (London, England), 1999. **13**: p. S61-72.

97. Deeks, S.G., et al., *HIV-1 protease inhibitors: a review for clinicians.* Jama, 1997. **277**(2): p. 145-153.

98. Li, Q., et al., *Long-term prophylaxis and pharmacokinetic evaluation of intramuscular Nano-and microparticle decoquinate in mice infected with P. berghei sporozoites.* Malaria research and treatment, 2017. **2017**.

99. Kohane, D.S., *Microparticles and nanoparticles for drug delivery.* Biotechnology and bioengineering, 2007. **96**(2): p. 203-209.

100. Raedler, L.A., *Aripiprazole lauroxil (Aristada): long-acting atypical antipsychotic injection approved for the treatment of patients with schizophrenia.* American health & drug benefits, 2016. **9**(Spec Feature): p. 40.

101. Agarwal, H.K., et al., *Emtricitabine prodrugs with improved anti-HIV activity and cellular uptake.* Molecular pharmaceutics, 2013. **10**(2): p. 467-476.

102. Dumortier, G., et al., *A review of poloxamer 407 pharmaceutical and pharmacological characteristics.* Pharmaceutical research, 2006. **23**(12): p. 2709-2728.

103. Doshi, N. and S. Mitragotri, *Macrophages recognize size and shape of their targets.* PloS one, 2010. **5**(4): p. e10051.

104. Nowacek, A.S., et al., *Analyses of nanoformulated antiretroviral drug charge, size, shape and content for uptake, drug release and antiviral activities in human monocyte-derived macrophages.* Journal of controlled release, 2011. **150**(2): p. 204-211.

105. Gratton, S.E., et al., *The effect of particle design on cellular internalization pathways.* Proceedings of the National Academy of Sciences, 2008. **105**(33): p. 11613-11618.

106. Barr, S.D., et al., *HIV integration site selection: targeting in macrophages and the effects of different routes of viral entry.* Molecular Therapy, 2006. **14**(2): p. 218-225.

107. Duncan, C.J. and Q.J. Sattentau, *Viral determinants of HIV-1 macrophage tropism.* Viruses, 2011. **3**(11): p. 2255-2279.

108. Genis, P., et al., *Cytokines and arachidonic metabolites produced during human immunodeficiency virus (HIV)-infected macrophage-astroglia interactions: implications for the neuropathogenesis of HIV disease.* Journal of Experimental Medicine, 1992. **176**(6): p. 1703-1718.

109. UNWALLA, H. and A.C. BANERJEA, *Inhibition of HIV-1 gene expression by novel macrophage-tropic DNA enzymes targeted to cleave HIV-1 TAT/Rev RNA.* Biochemical Journal, 2001. **357**(1): p. 147-155.

110. Kumar, A., W. Abbas, and G. Herbein, *HIV-1 latency in monocytes/macrophages.* Viruses, 2014. **6**(4): p. 1837-1860.

111. Sattentau, Q.J. and M. Stevenson, *Macrophages and HIV-1: An Unhealthy Constellation.* Cell host & microbe, 2016. **19**(3): p. 304-310.

112. Bahar, F.G., et al., *Species difference of esterase expression and hydrolase activity in plasma.* Journal of pharmaceutical sciences, 2012. **101**(10): p. 3979-3988.

113. Reimann, K.A., et al., *A chimeric simian/human immunodeficiency virus expressing a primary patient human immunodeficiency virus type 1 isolate env causes an AIDS-like disease after in vivo passage in rhesus monkeys.* Journal of virology, 1996. **70**(10): p. 6922-6928.

114. Nischang, M., et al., *Modeling HIV infection and therapies in humanized mice.* Swiss medical weekly, 2012. **142**(2728).

115. Mosier, D., et al., *Rapid loss of CD4+ T cells in human-PBL-SCID mice by noncytopathic HIV isolates.* Science, 1993. **260**(5108): p. 689-692.

116. Hoffmann-Fezer, G., et al., *Immunohistology and immunocytology of human T-cell chimerism and graft- versus-host disease in SCID mice.* Blood, 1993. **81**(12): p. 3440-3448.

117. Brainard, D.M., et al., *Induction of robust cellular and humoral virus-specific adaptive immune responses in human immunodeficiency virus-infected humanized BLT mice.* J Virol, 2009. **83**(14): p. 7305-21.

118. Gorantla, S., et al., *CD8+ cell depletion accelerates HIV-1 immunopathology in humanized mice.* The Journal of Immunology, 2010. **184**(12): p. 7082-7091.

119. Gorantla, S., et al., *Human immunodeficiency virus type 1 pathobiology studied in humanized BALB/c-Rag2−/− γc−/− mice.* Journal of virology, 2007. **81**(6): p. 2700-2712.

120. Araínga, M., et al., *HIV-1 cellular and tissue replication patterns in infected humanized mice.* Scientific reports, 2016. **6**: p. 23513.

121. Akkina, R., *New generation humanized mice for virus research: comparative aspects and future prospects.* Virology, 2013. **435**(1): p. 14-28.

122. Heredia, A., et al., *Monotherapy with either dolutegravir or raltegravir fails to durably suppress HIV viraemia in humanized mice.* Journal of Antimicrobial Chemotherapy, 2017. **72**(9): p. 2570-2573.

123. Pino, S., et al., *Development of novel major histocompatibility complex class I and class II-deficient NOD-SCID IL2R gamma chain knockout mice for modeling human xenogeneic graft-versus-host disease*, in *Mouse Models for Drug Discovery*. 2010, Springer. p. 105-117.

124. Wijting, I., et al., *Dolutegravir as maintenance monotherapy for HIV (DOMONO): a phase 2, randomised non-inferiority trial.* The Lancet HIV, 2017. **4**(12): p. e547-e554.

125. Watanabe, S., et al., *Hematopoietic stem cell–engrafted NOD/SCID/IL2Rγnull mice develop human lymphoid systems and induce long-lasting HIV-1 infection with specific humoral immune responses.* Blood, 2007. **109**(1): p. 212-218.

126. Agrahari, V., et al., *Stimuli-sensitive thiolated hyaluronic acid based nanofibers: synthesis, preclinical safety and in vitro anti-HIV activity.* Nanomedicine, 2016. **11**(22): p. 2935-2958.

127. Dutta, T., M. Garg, and N.K. Jain, *Targeting of efavirenz loaded tuftsin conjugated poly (propyleneimine) dendrimers to HIV infected macrophages in vitro.* European journal of pharmaceutical sciences, 2008. **34**(2-3): p. 181-189.

128. Endsley, A.N. and R.J. Ho, *Enhanced anti-HIV efficacy of Indinavir after inclusion in CD4 targeted lipid nanoparticles.* Journal of acquired immune deficiency syndromes (1999), 2012. **61**(4): p. 417.